LAWRENCE
LIVERMORE
NATIONAL
LABORATORY

LLNL-JRNL-834535

Three-dimensional Modeling of Plasma Edge Transport and Divertor Fluxes During Application of Resonant Magnetic Perturbations on ITER

O. Schmitz, M. Becoulet, P. Cahyna, T. E. Evans, Y. Feng, H. Freichs, A. Loarte, R. A. Pitts, D. Reiser, M. E. Fenstermacher

April 28, 2022

Nuclear Fusion

Disclaimer

This document was prepared as an account of work sponsored by an agency of the United States government. Neither the United States government nor Lawrence Livermore National Security, LLC, nor any of their employees makes any warranty, expressed or implied, or assumes any legal liability or responsibility for the accuracy, completeness, or usefulness of any information, apparatus, product, or process disclosed, or represents that its use would not infringe privately owned rights. Reference herein to any specific commercial product, process, or service by trade name, trademark, manufacturer, or otherwise does not necessarily constitute or imply its endorsement, recommendation, or favoring by the United States government or Lawrence Livermore National Security, LLC. The views and opinions of authors expressed herein do not necessarily state or reflect those of the United States government or Lawrence Livermore National Security, LLC, and shall not be used for advertising or product endorsement purposes.

Three-dimensional modeling of plasma edge transport and divertor fluxes during application of resonant magnetic perturbations on ITER

O. Schmitz[1], M. Becoulet[2], P. Cahyna[3], T.E. Evans[4], Y. Feng[5], H. Frerichs[1], A. Loarte[6], R.A. Pitts[6], D. Reiser[7], M.E. Fenstermacher[7], D. Harting[8], A. Kirschner[8], A. Kukushkin[9], T. Lunt[5], G. Saibene[9], D. Reiter[8], U. Samm[8], S. Wiesen[8]

[1] University of Wisconsin - Madison, Department of Engineering Physics, 53706 Madison, Wisconsin, USA
[2]CEA/IRFM, Cadarache, 13108 St. Paul-lez-Durance Cedex, France
[3]IPP AS CR, Za Slovankou 3, 18200 Prague 8, Czech Republik
[4]General Atomics, P.O. Box 85608, San Diego, California 92186-5608, USA
[5]Max Planck Institute for Plasma Physics, Association IPP-EURATOM, 17491 Greifswald, Germany
[6]ITER Organization, Route de Vinon-sur-Verdon, CS 90 04, 613067 St. Paul Lez Durance Cedex, France
[7] Lawrence Livermore National Laboratory, Livermore, California 94550, USA
[8]Institut für Energieforschung - Plasmaphysik, Forschungszentrum Jülich GmbH, 52425 Juelich, Germany
[9]*Present address:* NRC "Kurchatov Institute", Moscow 123182 and National Research Nuclear University MEPhI, Moscow 115409, Russia
[9]Fusion for Energy Joint Undertaking, Barcelona, Spain

E-mail: `oschmitz@wisc.edu`

Abstract. Results from three-dimensional modeling of plasma edge transport and plasma-wall interactions during application of resonant magnetic perturbation fields for control of edge-localized modes in the ITER standard 15 MA Q=10 H-mode are presented. The full 3-D plasma fluid and kinetic neutral transport code EMC3-EIRENE is used. Five characteristic perturbed magnetic topologies are considered. Two perturbation field amplitudes at full and half of the ITER ELM control coil current capability using the vacuum approximation are compared to a case including a strongly screening plasma response. In addition, a vacuum field case at high q_{95}, i.e. increased magnetic shear has been modeled.

Formation of a three-dimensional plasma boundary is seen for all five perturbed magnetic topologies. The resonant field amplitudes and the effective radial magnetic field at the separatrix define the shape and extension of the 3-D plasma boundary. Opening of the magnetic field lines from inside of the separatrix establishes scrape-off layer-like channels of direct parallel particle and heat flux towards the divertor yielding reduction of the main plasma thermal and particle confinement. This impact on confinement is most accentuated at full RMP current and is strongly reduced when screened RMP fields are considered as well as for the reduced coil current cases.

The divertor fluxes are redirected into a three-dimensional pattern of helical magnetic footprints on the divertor target tiles. At maximum perturbation strength, these fingers stretch out as far as $60cm$ across the divertor targets, yielding heat flux spreading and reduction of peak heat fluxes by 30%. However, at the same time substantial and highly localized heat fluxes reach divertor areas well outside of the axisymmetric power flux decay profile. Reduced RMP amplitudes due to screening or reduced RMP coil current yields reduction of the width of the divertor flux spreading to about $20 - 25cm$ and cause increased peak heat fluxes back to values similar to the axisymmetric case. The dependencies of these features on the divertor recycling regime and the perpendicular transport assumptions as well as toroidal averaged effects mimicking rotation of the RMP field are discussed in the paper.

1. Introduction

Application of resonant magnetic perturbation (RMP) fields is one of the two options for control of large type-I edge localized modes (ELMs) considered for ITER [1, 2, 3, 4]. During application of RMPs to achieve ELM suppression at DIII-D [5, 6] the redistribution of the plasma fluxes to plasma-facing components (PFCs) into a three-dimensional pattern was measured [7, 8, 9]. This has also been observed reliably during RMP application on several other devices [10, 11, 12, 13, 14, 15, 16]. This general and very reproducible effect is exemplified for the DIII-D case in figure 1. Here, the boundary light emission in two different wavelengths of carbon and hydrogen is shown during an RMP ELM suppressed H-mode plasma. A clear three-dimensional (3-D) distortion of the separatrix is visible in the tangential view [17] causing a striated hydrogen emission pattern on the divertor targets, which corresponds to the intersection of a helical structure with the divertor surface. The helicity of the divertor flux pattern is not clearly visible here because of the limited toroidal coverage of the camera. However, full 360 degree imaging of the 3-D divertor heat flux footprints at NSTX has demonstrated its helical nature with RMP fields [13]. Additional experimental evidence for the formation of a 3-D plasma boundary in DIII-D is discussed in [7, 8, 9, 18, 19, 20, 21].

This visible 3-D distortion of the plasma structure at the separatrix and on the divertor target is a result of a non-linear perturbation of the separatrix generated by the X-point in plasmas with a singular poloidal field null-point in the equilibrium magnetic field [22, 23, 24, 25]. The application of RMP fields causes the decomposition of the separatrix into a set of stable and unstable manifolds which form a complex, 3-D mesh at the X-point [18, 26, 27, 28]. This results in the formation of helical magnetic finger-like structures inducing a helical, 3-D magnetic footprint on the divertor target plates, which has been evaluated also for ITER [7, 29]. Recently, the overall 3-D distortion of the plasma boundary outside of the divertor has also been studied [30, 31], as well as the impact of the applied RMP fields on energetic particle confinement [32]. These studies emphasize the importance of understanding 3-D edge transport and PWI in tokamaks

when RMP fields are applied for edge stability control.

One key question regarding the application of RMP fields for ELM control in ITER [2, 7, 33] is the associated 3-D pattern of the plasma fluxes to plasma-facing components (PFCs) and the resulting plasma-wall interactions (PWI) since both deviate from the axisymmetric assumptions in modeling attempts for the ITER divertor design [34, 35]. This in fact represents a significant challenge, since several basic assumptions for the required 3-D transport modeling do not have a complete physics basis even for present experiments in axisymmetric situations. This concerns in particular the electromagnetic response of the ITER plasma, as a highly conductive medium, to the externally applied RMP fields [36] and the transport physics in the high temperature, very low collisionality plasmas expected in ITER. Modeling of the 3-D edge plasma transport when RMP fields are applied thus requires appropriate MHD and 3-D transport models to be available. In this paper, we present a first attempt to examine the likely effects of RMP ELM control on edge transport and PWI at ITER. This represents a substantial challenge for existing edge modeling tools, considering the ITER plasma size and unprecedented high core and edge/pedestal plasma temperature and density coupled to a partially detached divertor with high level of radiative energy losses to control power fluxes to the divertor targets [34, 35]. The limitations of the tools used for the study presented with respect to these challenges will be discussed.

The paper is organized as follows. First, the modeling tools will be introduced and the magnetic field topologies considered will be discussed in section 2. In section 3, an overview is provided on the transport features of the 3-D boundary induced, including the 3-D divertor flux footprints. In section 4, the impact of the RMP fields on the particle balance in all magnetic topologies considered is discussed, including the impact of the RMP fields on the divertor recycling regime. A concern for ITER is that the non-axisymmetric nature of heat fluxes to the divertor targets in the presence of RMPs will lead to additional fatigue stress in the divertor components and 3-D material erosion of the divertor surface. Rotation of the RMP field is thus being considered as an option to smear out heat and particle fluxes. A toroidally averaged analysis of the 3-D modeling results is presented in section 5 in order to mimic toroidally averaged fluxes resulting from such a rotation. In section 6, the role of the perpendicular transport assumption on the modeling trends is analyzed and, in section 7, a coil fault case is discussed in view of possible further 3-D distortion of the divertor heat and particle fluxes due to malfunctioning coils. The results are summarized and discussed with respect to the consequences for ITER and further modeling enhancements required in section 8.

2. Modeling assumptions and magnetic topologies considered

2.1. Plasma equilibrium and RMP coil setup

The reference plasma equilibrium for our modeling corresponds to the ITER Q=10 H-mode scenario with a plasma current $I_P = 15MA$, toroidal field of $B_T = 5.3T$ and a resulting safety factor $q_{95} = 3.2$. The equilibrium used in the modelling is a marginally MHD stable solution as a representative case just before ELMs are destabilized with a pedestal electron temperature of $T_e = 4.5keV$ [37]. In addition, we have also considered a lower plasma current H-mode scenario with higher $q_{95} = 4.5$. This case also works as a representative equilibrium for the possible conditions for H-mode access in the current ramp-up/down phases of the reference Q=10 scenario. The higher q_{95} is anticipated to change the shape of the 3-D plasma boundary structure as well as the internal transport features due to increased magnetic shear [38] and resonant transport effects if stochastic transport prevails [39, 40].

The general setup of the ITER ELM control coil set and of the two plasma equilibrium shapes addressed is illustrated in figure 2. The structure of the 3-D ELM control field considered in our studies has a toroidal mode number n=3 and two levels of currents I_C in the ELM control coils were used for the 15MA case, i.e. $I_C = 90kAt$ (maximum design value) and $I_C = 45kAt$. The phasing between the $n = 3$ harmonic fields created by the three rows of ELM control coils was optimized for maximum radial extension of the vacuum magnetic island overlap in an accompanying study presented in [3, 29]. This analysis was done using the vacuum approximation, i.e. a linear superposition of the unperturbed plasma equilibrium and the RMP magnetic field components. In order to address the possible impact of a plasma response to the external RMP field on plasma edge transport and PWI, a plasma response which strongly shields most of the interior resonant components has been used based on the following analysis of generic plasma response mechanisms in the ITER 15 MA, $Q_{DT} = 10$ H-mode reference scenario.

2.2. Plasma response assumptions and screening solution implemented

Two MHD codes which consider the problem in cylindrical geometry have been used: the 4-fluid, drift-kinetic code ATTEMPT [41, 42] and the 4-fluid, non-linear MHD code RMHD [38, 43]. Both models and the modeling results have been compared. The main deviation in the physics models contained in the ATTEMPT code is that toroidal rotation and perpendicular flows, i.e. parallel advection in general, are not included. In addition, neoclassical toroidal viscosity, which is incorporated in RMHD, is also absent in ATTEMPT. Hence, the ATTEMPT code approaches the diamagnetic limit of the RMHD code. Another important difference between these codes is that the plasma temperature is a radially constant quantity in ATTEMPT so that the pressure gradient is determined entirely by the density. The evaluation of plasma response for ITER with these two models has highlighted the following dominant physics mechanisms (more

details for the RMHD studies can be found in [38]):

- Diamagnetic screening by steep pressure gradients and flows in the plasma edge: due to the steep pressure gradients in the H-mode pedestal region, the components of the plasma flow perpendicular to the magnetic field, including ion and electron diamagnetic rotation, play an essential role in the screening of the applied resonant fields by the plasma. Variation of the pedestal parameters has shown that the diamagnetic rotation is the main contributor to the screening in the plasma edge where plasma flows are small and resistivity increases.
- Parametric dependencies: the level of plasma screening increases with decreasing resistivity, higher plasma toroidal rotation and for smaller RMPs amplitude due to a smaller decrease of plasma toroidal rotation as inferred with RMHD. Typically, the penetration of resonant fields into the confined plasma occurs in a narrow region near the separatrix due to a higher resistivity and the locally small values in the electron perpendicular drift velocities which prevent the occurrence of screening.
- Dependence on q-profile: for simulations in which the q-profile is matched between toroidal and cylindrical approximations - leading to realistic radial positions of resonances of the edge harmonics m=7:11 in the cylindrical approximation - externally applied n=3 resonant fields are found to penetrate into the confined plasma and to form an ergodic edge magnetic field region in ITER. The perpendicular plasma velocity is strongly modified by the applied RMPs and is close to zero in the n=3 case, which is favorable for the penetration of resonant fields. When the current in the ELM control coils is applied with n=4 symmetry there is a strong screening of the external resonant fields and the ergodic region is limited to the very edge (approximately $\Psi_N > 0.96$ in normalized toroidal flux Ψ_N) even for $I_C = 90kAt$.

Based on this comparative analysis of the results obtained with ATTEMPT and RMHD, a solution representing the strongest shielding factors for the resonant modes of the applied external field as predicted by RMHD for $n = 4$ toroidal base mode was implemented. To do so, this strongly shielding plasma response solution was transferred into toroidal geometry using the plasma current sheath model described in [14, 44]. The real calculated shielding factors from RMHD were used and helical current sheaths were implemented into the plasma equilibrium - preserving $\nabla \cdot B = 0$ - such that all resonant modes with $n = 3, 6$ and $m < 8$ are strongly reduced and that all modes with $m > 7$ undergo vacuum-like field penetration. This results in an almost fully screened RMP amplitude for $\Psi_N \lesssim 0.96$ and vacuum-like penetration outside this flux surface. This leads to a reduction of the radial extension of the stochastic magnetic field line domain reduced from $\Delta\Psi_N \approx 35\%$ using the vacuum approximation to $\Delta\Psi_N \lesssim 5\%$ when plasma screening is included [38].

This approach, using a cylindrical model to calculate the shielding factors and then translating these shielding factors into toroidal geometry, introduces some ambiguities

related to the mapping of the plasma current density and safety factor profiles between cylindrical and toroidal geometries. These uncertainties in the plasma response model might have a substantial influence on the level of screening expected for ITER. Implementation of a more complete description of plasma response from MHD models in full toroidal geometry such as M3D-C1 [45] or JOREK [38, 46] in the EM3C-Eirene modeling is a matter of ongoing research. Initial results using the total field from these two full toroidal models ([46, 47]) shows similar impact on plasma edge transport and PWI with 3-D RMP fields applied when compared to the case of strong screening used here. The strong resonant screening response is also consistent with recent observations in poloidally diverted L-mode plasmas with RMP fields at DIII-D, where resonant screening yields a strongly reduced level of 3-D effects on the visible edge plasma structure and transport [9]. However, in other plasma conditions - e.g. high β_N H-mode - the amplification effects of resonant field components are found to counteract the resonant screening and might actually lead to increased geometrical extension of the 3-D plasma boundary [36, 45, 47, 48].

The importance of mixed plasma response featuring both resonant field screening and resonant field amplification [49, 50] has also been linked to the stability of the peeling-ballooning modes [51, 52] and recently been identified as a possible required condition to obtain ELM suppression at DIII-D [53, 54]. EM3C-Eirene studies for ITER incorporating such more complete plasma response description are on-going. The strong screening response, together with the two levels of ELM control coil current and variation of the magnetic shear addressed in the study discussed in this paper, represents a broad scan across possible solutions of the magnetic topology. In this regard, the intention with this paper is to scope out the possible range of impact of 3-D RMP fields for ELM control at ITER on plasma edge transport and PWI.

2.3. Overview on perturbed magnetic topologies considered

Figure 3 shows the perturbed magnetic field structure obtained by magnetic field line tracing for the ITER plasmas and ELM control current levels studied here. A strong stochastization of the 15 MA ITER plasma edge is seen in figure 3,a in the vacuum magnetic field structure for the maximum value of $I_c = 90kAt$. A chain of large magnetic islands is formed even at $\Psi_N \approx 0.55$ and the highly stochastic edge structure reaches in as far as $\Delta\Psi_N \approx 0.35$ from the unperturbed separatrix. As expected, the islands inside the confined plasma as well as the extension of the stochastic edge layer are significantly reduced to $\Delta\Psi_N \approx 5\%$ when the strongly shielding plasma response is considered a shown in figure 3.b. A similar effect is seen, when the ELM control current amplitude is reduced from $I_C = 90kAt$ to $I_C = 45kAt$ and vacuum RMP fields are used as shown in figure 3.c. The stochastic layer extension is reduced to $\Delta\Psi_N = 0.15$ because the island size on the interior resonant surfaces is strongly reduced. Larger

magnetic shear for the $q_{95} = 4.5$ plasma leads to a compression of the distance between resonant surfaces and to an increase of the remnant islands in the formerly dominant stochastic layer for $I_c = 45kAt$ (see figure 3.d). In this case the region outside $\Psi_N > 0.8$ is considered as quasi-stochastic due to the strong transport along the field line which takes place between the islands. A more systematic assessment of the stochastic layer characteristics in ITER is discussed in [29]. The vacuum magnetic topologies considered in this paper were selected of the basis on this extensive study.

2.4. The EMC3-EIRENE transport code package

For transport modeling, the EMC3-EIRENE [55, 56, 57] code package is used. EMC3 solves a set of reduced Braginskii fluid equations (Particle, Energy and Momentum) and is iteratively coupled to the 3D kinetic neutral transport code EIRENE [58]. The latter supplies the particle, energy and momentum sources and sinks from neutrals recycled at PFCs to the EM3C code. EM3C-EIRENE was recently adapted to 3-D modeling of the plasma edge transport during RMP ELM suppression experiments at DIII-D [59, 60, 61] and has been satisfactorily benchmarked with the SOLPS code [34] ‡ for axisymmetric ITER plasmas in attached divertor conditions [62]. The model has also been used for ITER startup limiter modeling [63] and has been employed successfully for analysis of 3-D edge transport and PWI in RMP ELM control experiments at ASDEX-Upgrade and NSTX [64, 65] and for RMP experiments at LHD [66, 67].

The initial ITER divertor regime modeled in our studies corresponds to a fully attached, medium recycling case at an intermediate density of $n_{ISB} = 5.0 \times 10^{19} m^{-3}$ at the inner simulation boundary (ISB), corresponding to $n_{sep} = 3.2 \times 10^{19} m^{-3}$ at the separatrix before RMP fields are applied. This regime is used in most of the paper to discuss generic features of 3-D edge transport and PWI with RMP fields at ITER. In addition, we have carried out variations of the target recycling flux in order to assess the impact of RMP fields on the divertor recycling regime and at the same time study 3-D divertor heat fluxes under high recycling, low temperature divertor conditions.

In this study, the code was pushed to the borders of its numerical stability, enabling access to cold divertor conditions characteristic of high recycling divertor conditions at $T_e \approx T_i \lesssim 10eV$. Dissipative divertor conditions with high radiation losses and partial detachment - the ITER reference divertor scenario for the Q=10, 15MA H-mode scenario - cannot yet be accessed. Work to improve the particle balance in EM3C-EIRENE allowing the treatment of volumetric particle sources and sinks required to model detached divertor conditions and improving its numerical stability is in progress [68]. Similarly, the proper treatment of impurities is required to model divertors plasmas with high radiative losses. This is not yet possible with EM3C-EIRENE in a numerically stable

‡ With SOLPS, we refer to the Scrape-Off Layer Plasma Simulation (SOLPS) suite version SOLPS-4.3, which was used at the time of the study presented as the standard version for ITER divertor modeling.

fashion for the ITER scenarios considered and the effects from RMP fields included, but is a matter of ongoing code development. Therefore, the first 3-D edge transport study for ITER presented in this paper is restricted to the medium to high recycling divertor regime where the EMC3-EIRENE code has been shown to be numerically stable. The study presented here therefore represents a scoping study in terms of both, the different magnetic topologies considered and the divertor regime just before onset of detachment governed by hydrogen ionization losses as dominant energy loss mechanism. Based on these constraints in the modeling approach, we present upper maxima for the divertor target heat fluxes and for the convective heat and particle flows in the RMP induced 3-D helical SOL.

The input power to the modeling domain in all cases modeled was $P_{SOL} = 100MW$, which is the typical level expected in ITER high Q_{DT} operation. Radial transport is described by radially and poloidally constant perpendicular diffusion coefficients for particles $D_\perp$ and heat $\chi_\perp$ in EMC3-EIRENE whose values were varied upwards from $0.4m^2/s$ to $1.2m^2/s$ for $D_\perp$ and $\chi_\perp = 3\times D_\perp$ as fixed ratio, respectively. The lower values of the transport coefficients are similar to those used in ITER $Q_{DT} = 10$ simulations corresponding to a SOL heat flux decay length $\lambda_q = 4mm$ [34, 35]. A core particle source Q_C was defined in this study inside of the ISB and varied in the range of $Q_C = 2.25 - 3.75 \times 10^{22}/s$. These values are required to maintain the target density at the ISB (n_{ISB}) during enhanced particle losses associated with RMP induced enhanced particle transport - called particle pump-out in experiment (see e.g. [5, 40, 74]). This level of Q_C is much is higher than the fueling associated with the ITER neutral beam injection at the full power ($\approx 2.0 \times 10^{20}\ at/s$), but less than 40% of the total ITER stationary pellet fueling capabilities ($\approx 1.0 \times 10^{23}\ at/s$).

3. Dependence of 3-D plasma boundary structure and transport on the magnetic field topology

3.1. 3-D plasma edge structure and thermal confinement

Figure 4 shows an overview of the plasma edge parameters for the five representative magnetic topologies described earlier. The electron temperature $T_e(R, Z)$ and the Mach number $M(R, Z)$ of the plasma flow along the magnetic field at toroidal position $\phi = 0\ deg$ are shown. The temperature maps visualize that for all cases where RMP fields are applied, a 3-D plasma boundary is formed with the appearance of high temperature finger structures at the X-point. These reach out towards the divertor target and intersect them in some cases at locations far away along the target from the axisymmetric strike point location. The result is a helical divertor target heat and particle flux pattern producing significant 3-D divertor power loads outside the divertor power decay length of $\approx 5 - 10cm$ typical for the $15MA$, $Q_{DT} = 10$ standard H-mode scenario.

When plasma screening is included, the radial reach out of the plasma fingers is reduced and the outer lobes no longer reach the divertor target as seen in figure 4.c. A very similar trend is found (see figure 4,d) when I_C was reduced to $45kAt$, which is the minimum value required to obtain island overlap at $\Psi_N = 0.87$ - the heuristic scaling requirement for RMP ELM suppression between DIII-D and ITER [29, 69]. Increasing the magnetic shear at the separatrix by increasing q_{95}, while maintaining $I_c = 45kAt$, leads to a very dense mesh of high temperature fingers but with short radial reach out - most of which do not reach the divertor targets as seen in figure 4,e.

The modeling with EM3C-Eirene shows that the application of 3-D fields can have a large effect on the plasma thermal confinement and that the size of the effect depends on the amplitude of the effective RMP field. The comparison of the axisymmetric case (figure 4.a) with the case of RMP fields with $I_C = 90kAt$ in the vacuum approximation (figure 4,b) shows a sizable decrease of the plasma thermal confinement, reflected in the reduction of $T_e = 4keV \rightarrow 1.8keV$ at the ISB. This is a consequence of the strong perturbation to the edge magnetic field structure evaluated in the vacuum approximation which, causes a wide extension of the confined plasma to be connected along open field lines to the PFCs [3, 29]. This leads to a high parallel heat transport along the open, perturbed field lines and thus to a large decrease of the plasma temperature in this previously confined plasma region.

It is important to note that such strong (factor 2) drop of the thermal plasma confinement was not seen in experiment, where only small effects on the thermal confinement are observed (on the level of a $\approx 10 - 20\%$ reduction compared to the no-RMP profiles) [39, 40]. One of the potential explanations is that the plasma response to the applied external RMP fields reduces the amplitudes of the resonant components in the plasma and thus the extension of the region with open field lines at the the plasma edge. This has been evaluated by including plasma screening as described before. The results of the EMC3-EIRENE modeling for such conditions are shown in figure 4.c for $T_e(R, Z)$. The strong degradation of the thermal confinement is eliminated to leave a reduction of $\Delta T_e \approx 10 - 15\%$ only when compared to the axisymmetric situation. Reducing I_C to $45kAt$ and using the vacuum field resonant amplitudes also leads to a smaller temperature drop of only $\Delta T \approx 20\%$ when 3-D fields are applied (see figure 4.d). The much more moderate reduction in ΔT for both the screened case and the case at $I_C = 45kAt$ is due to the reduced width of the stochastic layer in both cases. This level of ΔT is more compatible with observations during full ELM suppression at DIII-D, as discussed in [39, 40, 70]. Similarly, for the higher q_{95} case (see figure 4.e) with $I_C = 45kAt$, the radial extension of the perturbed open field line domain is only $\Delta\Psi_N \approx 20\%$ and consequently $\Delta T_e \approx 25\%$ is comparably small. In addition to the effect of a much smaller stochastic layer width for the higher q_{95} value, the magnetic fingers at the X-point form a dense mesh with less radial reach out which in some cases do not intersect the divertor targets. As a consequence, the effective connection length

of the field lines in the open field line layer increases and this leads to a reduction of the direct parallel energy losses.

3.2. 3-D helical scrape-off layer flows

The application of RMP fields has a strong impact on the sonic flow pattern for all four magnetic topologies considered. This is shown in figures 4.f-j. For the axisymmetric ITER case shown in figure 4.f, the usual 2D flow pattern at the plasma edge is found: very low values of the parallel flow Mach number are seen in the confined plasma and the main Scrape-Off Layer (SOL) region. The plasma flow speeds reach ion sound velocity at the targets as required by the sheath Bohm boundary condition used in the EMC3-EIRENE model. It is important to note that reversal of the plasma flow is seen near the inner and outer strike points for the axisymmetric case. This is the result of the highly localized particle source from the ion influx recycling pattern, which is typical of vertical target divertors [71], and is discussed in more detail as part of the EMC3-Eirene/SOLPS benchmark in [62].

When 3-D RMP fields are applied, a checkerboard pattern of counter streaming plasma parallel flow channels is obtained around the X-point which extends deep into the confined plasma as seen in figures 4g-j. The inwards extension of the counter-flow pattern is determined by the effective resonant amplitude of the applied RMP fields. The generic mechanisms behind this 3-D flow structure are analyzed in [28] on the example of DIII-D. Here, we discuss the impact on edge transport during RMP field application for ELM control at ITER. Outside the separatrix, in the region away from the divertor such as the main chamber plasma top, counter streaming flows can be seen in neighboring helical finger structures. Near the divertor this is modified to regions of strong and weak flow in the same direction, as expected from the general flow pattern imposed by the Bohm boundary conditions at the two divertor targets. The typical plasma parallel velocity in these counter flowing channels can be as high as $M = 0.3 - 0.5$ even for positions located inside the separatrix in the axisymmetric situation.

Depending on the level of the applied RMP field and the resulting plasma screening, a substantial fraction of the field lines in the plasma region located inside the magnetic separatrix (for the axisymmetric situation) can become directly connected to the PFCs by the application of 3-D fields and thus cause the appearance of high parallel power and particle fluxes to material surfaces [12, 29]. In addition, field line mixing due to overlapping resonant island chains deeper inside of the plasma domain causes further direct magnetic connections of the confined plasma to the PFCs through cascading jumps between the resonant island chains [28] along relatively short connection length field lines (SOL-like)with $L_c = 50 - 80m$ in ITER. The 3-D magnetic flux bundles established by the RMP fields thus connect regions of the plasma with high plasma pressure (in the confined plasma) with regions where the plasma pressure is lower (SOL

and the vicinity of the PFCs) leading to the establishment of the 3D helical SOL flow pattern shown in figure 4.g-j [33]. The feature of counter streaming flow channels is a result of the shortest pathway to the PFC along the magnetic field line from the various poloidal domains. Details on how the checkerboard pattern of counter streaming flows is generated can be found in [28]. The plasma particle out-flux associated to these SOL like flows channels from inside of the separatrix is a likely contributor to the experimentally observed particle pump-out [5, 6, 40]. As described above, the real inward extension of the SOL flow structures depends strongly on the ELM control coil current amplitude and on the plasma response. We will discuss the dependence of the stationary particle confinement in EMC3-EIRENE modeling results on the RMP amplitude and the screening level in section 4.

3.3. 3-D divertor fluxes

The formation of a 3-D helical pattern of the divertor heat and particle fluxes is clearly seen for all the cases in which 3-D RMP fields are applied. This leads to the splitting of the strike point into three lobes (i.e. symmetric to the toroidal base mode of the applied 3-D RMP field) which channel substantial particle and power fluxes to the divertor targets. In figure 5, the divertor toroidal and poloidal heat and particle flux distributions at the outer target (OT) and inner target (IT) are shown from left to right in the same order as for figure 4. Qualitatively, the splitting width of both, heat and particle fluxes, is higher at the OT and smaller at the IT for all magnetic topologies considered. This is a consequence of the upward bending of the separatrix lobes at the high field side seen for example in the temperature pattern in figure 4. The separatrix lobes are stretched out substantially for the vacuum case at full current, but they are deflected towards the upper marginal X-point rather then intersecting the divertor target in the vicinity of the IT. Therefore, the heat and particle flux patterns show a narrower striated footprint on the IT then seen at the OT. We will focus on a more detailed discussion of the OT flux pattern, in order to assess the strongest effect for divertor flux splitting.

The maximum splitting width at the OT obtained in the modeling is about 60 cm for the 15 MA plasma equilibrium at $I_C = 90kAt$ using the vacuum approximation. The splitting is substantially reduced for the other magnetic topologies considered since the effective RMP fields are decreased either by I_C or by the inclusion of plasma screening. This is due to the decrease of the radial magnetic field at the separatrix which reduces the spreading of the separatrix fingers leading to a reduced splitting of the associated power and particle fluxes when they reach the divertor targets [9, 14, 44].

In the experiments at DIII-D, clear splitting of the divertor particle fluxes is observed when RMP fields are applied to suppress ELMs in low collisionality plasmas. However, only very low power fluxes are measured for the lobes reaching far away from the unperturbed strike point [7, 12, 19]. In contrast, the ITER EMC3-EIRENE simulations

show substantial power fluxes in all the three lobes with relatively long decay lengths, so that the power fluxes in regions well away from the unperturbed separatrix can be significant. Their magnitude depends on the effective amplitude of the RMP fields applied. Including plasma screening therefore leads to a concentration of the heat and particle fluxes in the lobes closer to the unperturbed separatrix as shown in figure 5 c and f. This is in qualitative agreement with the experimental trends as discussed in [70].

A quantitative comparison of the modeled heat and particle fluxes at the OT is shown in figure 6. Here, the heat and particle flux profiles along the outer divertor target are plotted at the toroidal angle $\phi = 0\,\mathrm{deg}$. The strike point splitting not only affects the level of heat and particle flux far away from the unperturbed separatrix strike line, but also the modeled peak heat $\hat{q}_{SP}$ and particle $\hat{\Gamma}_{SP}$ fluxes close to the unperturbed strike line location. Larger splitting leads to a higher heat flux spreading and thus reduced $\hat{q}_{SP}$ and $\hat{\Gamma}_{SP}$ since the level of SOL power input is kept constant in these simulations (100 MW). Therefore, for the case with 15 MA plasma and $I_C = 90kAt$ in the vacuum approximation, the peak heat flux at the outer divertor decreases down to $\hat{q}_{SP} = 10MWm^{-2}$ from a value of $\hat{q}_{SP} = 24MWm^{-2}$ for the axisymmetric case. For the other cases with lower effective RMP fields, the decrease of the peak heat flux is smaller ($\hat{q}_{SP} = 17MWm^{-2}$ for $I_C = 90kAt$ including plasma screening, $\hat{q} = 21MWm^{-2}$ for the vacuum case with $I_C = 45kAt$ and $\hat{q} = 19MWm^{-2}$ for the high q_{95} vacuum case with $I_C = 45kAt$). Simultaneously, the radial splitting of the power flux is reduced with the lobes reaching up to $\leq 25cm$ away from the unperturbed strike line for the screened case and the $I_C = 45kAt$ cases (cf. 60 cm for the $I_C = 90kAt$ vacuum case).

These results show as a general trend that the peak heat fluxes can be reduced by the 3-D fields with the real magnitude of the reduction depending on the level of plasma response or the applied RMP amplitude level. However, the heat flux is shifted away from the unperturbed strike line inside of the helical magnetic footprint pattern, and hence localized regions of peaked heat fluxes on areas of the divertor which is not designed to handle such heat flux levels can occur. This result is obtained in the modeling discussed so far with a fully attached divertor solution and the extent to which it may really occur in the partially detached, highly dissipative divertor solution at ITER needs to be assessed. However, the heat flux spreading seen in the modeling so far combined with possible facilitation of localized energy losses in the outer lobes as recently discussed for the DIII-D divertor during RMP ELM suppression [70] possibly aids the power handling in the ITER divertor. In this regard, the application of 3-D resonant fields could potentially be a feasible tool for the control of stationary power loads in view of the narrow power SOL decay lengths predicted for ITER [72, 73].

The striation of the divertor heat flux is also seen in the particle fluxes, as shown in figure 5 and 6. In this case, the level of particle flux obtained for the simulations when 3-D resonant fields are applied is lower than the axisymmetric solution because the level

of plasma recycling in the 3-D solutions is lower. This is a result of the particle balance in EMC3-EIRENE, which leads to a lower integrated divertor flux when 3-D fields are considered (unlike the integral divertor power flow which is the same in the two cases). This modeling result for the divertor particle flux and the dependence of the divertor recycling regime on the 3-D magnetic topology will be discussed in more detail in section 4.

4. Particle balance and divertor recycling regime with 3D fields

4.1. Particle balance and particle pump-out

The achievement of ELM suppression with 3-D RMP fields in low collisionality plasma experiments at DIII-D is typically accompanied by a reduction of the plasma density - called density pump-out[6, 39, 40]. The ITER modeling study presented here shows a similar effect, however not in form of a reduced plasma density but as an increased source level required to maintain a fixed density at the ISB. Since high plasma density is mandatory for ITER to maintain a high fusion gain, we keep the density fixed at the ISB for the various magnetic field topologies addressed. In order to resolve the impact on the particle confinement and identify the experimentally observed density pump-out, we must discuss the particle balance in terms of the relation of plasma sources and sinks and the actual particle confinement time. This will be addressed in this section.

For the modeled cases discussed so far in this paper, a fixed density at the ISB of $n_{ISB} = 5.0 \times 10^{19} m^{-3}$ was used. At fixed ISB density, the particle pump-out is seen as a change of the overall plasma source $Q_{tot} = Q_C + Q_{rec}$. We use EMC3-EIRENE such that Q_{tot} is provided from core fueling Q_c inside of the ISB and $Q_{rec} = \int \Gamma_{rec}$ as the integral recycling flux on the divertor targets $\int \Gamma_{rec}$. Here, Q_{rec} is adjusted in the iteration procedure of the model such that the particle balance matching the requested density at the ISB n_{ISB} is established.

This specific approach to maintain n_{ISB} has a consequence for the comparability of the heat flux result across the various magnetic topologies. If we keep Q_c fixed, Q_{rec} will increase linearly (linear recycling regime) or almost quadratically (high recycling regime) which can cause a substantial reduction of the divertor heat flux in particular in the 3-D helical footprint pattern [70]. Since in this first step of our analysis we target the investigation of the impact of the magnetic topology on the heat flux pattern, we want to avoid or at least mitigate this effect of the perturbed particle balance on the heat flux distribution. We therefore adjust Q_c to minimize the change of Q_{rec}. The combined increase of Q_{rec} and Q_c to maintain n_{ISB} is then a measure for the level of particle pump-out seen in the modeling result for each magnetic field topology. Table 1 provides an overview is given of Q_{rec}, the integral target heat flux $\int q$ the energy loss due to ionization of neutrals E_{io} and pumped fraction $\epsilon_P = Q_c/Q_{rec}$ of the divertor

particle flux of the simulations considered in this section.

No.	Scenario	$Q_{rec}[kA]$	$\int q_{target}[MW]$	$E_{io}[MW]$	ϵ_{pump}
1	no-RMP	281.5	94.41	5.49	0.012
2	vacuum, 90kAt	133.5	96.3	2.67	0.042
3	vacuum, 45 kAt	67.2	92.1	7.8	0.008
4	screened, 90 kAt, fixed density	16.2	90.18	9.81	0.33
5	screened, 90kAt, fixed flux	281.25	95.1	5.19	0.012
6	vacuum, high q_{95}, 45 kAt,	132.0	93.3	6.63	0.041

Table 1: Integrated divertor fluxes and power losses for all magnetic topologies considered in this paper.

The axisymmetric solution (No. 1) was obtained with a constant core particle source of $Q_C = 3600A = 2.25 \times 10^{22} particles/s$. For the RMP cases (No. 2-6), this value had to be increased to $Q_C = 5400A = 3.75 \times 10^{22} particles/s$ to maintain the same n_{ISB} for similar Q_{rec}. Both core fueling levels applied are well within the pellet fueling capabilities of ITER, but the increase required to compensate the higher particle out-flux from the core plasma when RMP fields are applied is noticeable (a 60% increase with respect to the axisymmetric solution). The adjustment of the total particle source by increasing Q_C in our modeling still leaves Q_{rec} as the actual adjustable particle source level by the iteration procedure in EMC3-EIRENE such that constant n_{ISB} is obtained. Hence, the eventual integrated target particle fluxes shown in table 1 still vary over a factor of 5. To explore the sensitivity of the results to the remaining change of Q_{rec}, two cases were considered for the screened magnetic field topology: one in which the density of the plasma is fixed (No. 4) and one in which the particle flux at the divertor target was fixed (No.5) to the same value of the axisymmetric solution. A factor of ≈ 20 reduction of Q_{rec} below the no-RMP reference value is seen, when n_{ISB} is kept constant at the elevated level of Q_C for the $I_C = 90kAt$ and $I_C = 45kAt$ vacuum field case. This means that the additional core fueling required for both vacuum cases is substantially higher then that required for the screened case and emphasizes that the perturbation of the particle balance due to the 3-D plasma boundary structure potentially has significant implications for the plasma neutral fueling scheme. The actual source level again depends on the resonant field amplitudes required to obtain ELM suppression and on the plasma response to this RMP field level.

In order to quantify the impact of RMP fields on the particle balance, a single reservoir particle balance model as applied for analysis of RMP particle transport experiments at TEXTOR [39] and DIII-D [74] was applied to the EM3C results. Because a converged EMC3-EIRENE solution represents a stationary plasma/neutral state, the time dependence of the particle balance vanishes ($\frac{dN_{tot}}{dt} = 0$) and the solution of the single reservoir

model can be simplified to $\frac{N_{tot}}{\tau_P} = Q_{rec}$. Here, τ_P is the particle confinement time which is a quantitative measure for the level of particle pump-out seen in a converged, i.e. stationary EMC3-EIRENE solution. A constant value of the recycling coefficient ($R < 1$) is assumed on all the recycling surfaces and the particles removed Γ_{pump} are injected in the simulations by the core source Q_C coming from the inside of the ISB. In stationary conditions $Q_C = \Gamma_{pump}$ and the ratio $\epsilon = Q_C/Q_{rec}$ provides the the pumping fraction of the recycling flux wich is displayed in table 1. The assumption of a core particle source at the position of the ISB corresponds to a realistic situation for ITER with pellet fueling only if the position of the inner boundary in the simulations $\Psi_N(ISB)$ is not deeper than the pellet penetration depth inside of the plasma. This is fulfilled for the cases which account for screening in table 1 (cases No. 4 and 5).

For all perturbed topologies considered, the application of 3-D RMP field leads to an increase of the required Q_{tot} compared to the axisymmetric, no-RMP case. However, for the value of Q_c used and the boundary condition of fixed n_{ISB}, a decrease of Q_{rec} is seen in the EMC3-EIRENE simulations compared to the value in the axisymmetric situation. This is due to the need to increase Q_c by about 50% for the two RMP cases to keep the same n_{ISB} as for the axisymmetric situation and to maintain a moderate change in Q_{rec}. While the increase in Q_c is sufficient to compensate the additional confined plasma out-flux created by the 3-D edge magnetic field structure - it also causes a decrease in the target recycling flux in the EM3C-Eirene simulations due to the modeling assumptions applied.

A strong impact of RMP field screening on the particle balance can be seen when comparing the exhaust fractions ϵ_P from cases No. 2 and No. 4. The core particle source Q_c was the same for both cases and a factor of 20 lower value for $\int \Gamma_{target}$ is required for the screens case at fixed n_{ISB}. Accordingly, the relative amount of particle source which is supplied from the core domain is a factor of > 10 lower for the screened case than for the $I_C = 90kAt$ vacuum RMP case. This shows that the total particle source from the vacuum field case at $I_C = 90kAt$ in vacuum to the screened case at the same nominal I_C value was largely reduced. Hence, the density pump-out for the screened case (No. 5) is much weaker than for the vacuum RMP case at $I_C = 90kAt$ (No. 2) or $I_C = 45kAt$ (No. 3) - all using fixed n_{ISB} as boundary condition. The reason for the particle pump-out within the modeling approach of EMC3-EIRENE is the strongly reduced inward extension of direct parallel flow channels from $\Delta\Psi_N \approx 35\%$ in vacuum at full current to $\Delta\Psi_N \approx 15\%$ only for the screened case [40] as discussed before.

In order to quantify the effect of 3-D fields on the plasma particle confinement time it is important to maintain comparable divertor recycling conditions (i.e. particle flux and pumped flux). This has been achieved by carrying out a simulation (including plasma screening, case No. 5 in table 1) in which the value of the divertor particle flux is used as boundary condition when RMP fields are considered and set to the same value of the

axisymmetric case (case No. 1). Analysis of these simulations show that the helical SOL flow pattern created by the RMP fields and the associated increased particle outflow from the plasma leads to a decrease of $\Delta\tau_P$ relative to the no-RMP case of $\Delta\tau_P = 35\%$ for the case with full $I_C = 90kAt$, $\Delta\tau_P = 16\%$ for the case with full $I_C = 45kAt$ and $\Delta\tau_P = 20\%$ for case including plasma screening. The actual magnetic field topology defined by the RMP amplitude required to suppress ELMs at ITER and the plasma response will therefore define the modification of the particle balance and hence the level of increased fueling and tritium throughput.

4.2. Particle balance and divertor recycling regime

In the case of the fully attached divertor concerned so far by these simulations, the losses due to neutral recycling processes are much lower than the SOL power input (see table 1). As a consequence, the choice of boundary conditions for the modeling of power balance plays only a minor role. This is shown for the total heat flux reaching the divertor target for the screened RMP case (No. 4 and No. 5 in table 1) in figure 7.

Although the magnitudes of the peak heat fluxes are similar for the two cases, the spatial structure of the heat and particle flux profiles is different at various toroidal locations. This is caused by the much higher divertor densities for the simulation which uses Q_{rec} as boundary condition (case No. 5 with outer divertor density $n_{OSP} = 8.2 \times 10^{19} m^{-3}$) than the case in which control of n_{ISB} (case No. 4 with outer divertor density $n_{OSP} = 8.0 \times 10^{18} m^{-3}$) is used. The strong impact of the choice of this boundary condition on the divertor target flux is reflected in the order of magnitude difference between the values of the particle flux shown in figure 7 for these two cases. The larger divertor densities in case No. 5 versus No. 4 affect the local ionization of neutrals at the 3-D plasma fingers in the divertor region leading to narrower structures of the target particle flux in the lobes away from the unperturbed separatrix strike point for case No. 5. This, modeled in attached, linear recycling divertor conditions, leads to a similar change in the heat flux deposition profiles.

Thus we conclude that for these divertor conditions, the neutral recycling losses are too small to affect the total and the peak divertor fluxes. However, changes to the ionization pattern associated with the increased density are large enough to cause measurable changes in the spatial structure of the divertor target particle and heat fluxes. This is a very important finding and demonstrates that significant effects on the spatial distribution of particle and power fluxes are expected to occur for the high density/high radiation divertor conditions with which ITER must operate for the control of divertor power loads. Modeling of these ITER divertor relevant conditions requires an upgrade (in progress) of the particle balance treatment in EM3C-EIRENE.

To further investigate the divertor recycling behavior with RMP fields in comparison

with the axisymmetric situation, a divertor recycling flux scan was performed from a sheath limited divertor regime with divertor densities of $1 \times 10^{19} m^{-3}$ to a high recycling divertor with divertor densities of $6 \times 10^{19} m^{-3}$ and low divertor temperatures (5-10 eV), but still in the attached divertor regime. The strongly screened RMP case was used for this scan as it still provides significant 3-D effects, but because of the reduced width of the stochastic layer, the prominent and probably exaggerated (when comparing to experiments) effect of the direct SOL-like connection from the interior and hence a strong particle pump-out is mitigated. As shown in figure 8, overall a larger recycling flux is required when RMP fields are applied compared to the axisymmetric situation to obtain a given upstream density n_{ISB}. This is consistent with the decreased τ_P found when RMP fields are applied as discussed earlier and also with the more localized ionization pattern at the divertor (and thus reduced penetration of neutrals into the confined plasma) shown in figure 7.

It is important to note that the cases considered include screening of the applied external fields and thus only a largely reduced depth of the confined plasma is affected. Despite this, the structure of strong parallel flows (co and counter streaming) created in the confined plasma is found to have a major effect on the particle balance as illustrated in figure 8. In addition, the dense mesh of counter streaming flow channels created by the 3-D fields at the plasma edge represents a significant momentum sink to the plasma ions flowing out from the confined plasma, but also to the ions which are created at the plasma edge by the ionization of recycling neutrals. The balance between the inward directed particle fluxes driven by thermal-forces (parallel gradients in collisionality) and frictional forces is perturbed by the 3-D flow pattern and this found to reduce the efficiency of fueling by the ionization of recycled neutrals at the plasma edge as studied numerically at ASDEX-Upgrade in [75] and also seen in TEXTOR experiments [39].

The preceding discussion of the impact of the RMP fields on the particle balance has highlighted the strong perturbation to the plasma source-sink relation induced by the 3-D helical SOL flow structure induced. This new 3-D SOL extends into the formerly confined plasma region and hence enhances outward particle transport and at the same time it reduces plasma fueling from recycled neutral sources. However, while providing a self-consistent explanation of the loss in global particle confinement within the EMC3-EIRENE modeling framework, these are not the only mechanisms which can contribute to the experimentally observed changes of particle confinement. Other mechanisms for instance that have been identified to play a role in the experiments are the reduction of radial electric field shear [39, 76, 77], possibly causing the measured increase in the turbulence driven particle flux [53, 78], or the impact of magnetic flutter on ambipolar particle confinement [79, 80]. While the magnitude of these or other mechanisms may be important in present experiments, their extrapolation to ITER requires a self-consistent treatment of the transport channels together with the neutral particle sources and sinks. Using EMC3-EIRENE, these dedicated transport aspects driving radial par-

ticle and heat transport are introduced as radially and poloidally constant perpendicular transport coefficients $D_\perp$ and $\chi_\perp$. They can be adapted to different values including a radial dependence to account for new findings on the radial transport mechanism [70]. In the study presented here, radially and poloidally constant transport coefficients were used. This numerical analysis supports that the identified effects of RMP fields on particle confinement (enhanced particle losses due to particles fluxes from the main plasma to the PFCs along the field lines and reduced fueling efficiency of recycling neutrals due to the associated 3-D edge plasma and flow structure) are likely to provide a lower limit for the magnitude of the effects of RMP fields on core particle confinement in ITER. Further quantitative analysis of the impact of the applied RMP fields on particle transport and fueling - in particular for pellet fueling - will be performed in future studies.

As shown in figure 8, the divertor conditions change with increasing recycling flux in a very comparable way in the screened RMP case compared to the axisymmetric case, despite the strong modification of the recycling behavior by the application of RMP fields. Divertor densities of up to $6 \times 10^{20} m^{-3}$ are obtained for the highest divertor target recycling fluxes and correspondingly the divertor temperatures decrease to values of $T_e = 6eV$ and $T_i = 11eV$ with increased neutral ionization losses at the divertor. This divertor regime is at the threshold for the onset of volume recombination as localized domains in the divertor show temperatures at $2eV$ an below. Due to the limitations in the present particle balance model in EM3C-Eirene described in section 4.1, it is not yet possible to model lower divertor temperature/detached divertor conditions with RMP fields for ITER using EMC3-EIRENE. The missing capabilities of EMC3-EIRENE are presently being implemented and it is planned to continue these studies once an upgraded version of the code is available.

5. Toroidally averaged heat and particle loads onto the ITER divertor

The toroidally asymmetric divertor target heat and particle fluxes created by the application of RMP fields can potentially lead to a long-term, non-toroidally uniform erosion pattern of the divertor target material. A proposed solution to average out such non-toroidally uniform erosion in ITER and also to make use of the heat flux distribution in the helical target footprints to spread heat flux across a larger divertor area is the rotation of the RMP field applied [2]. This can be achieved by the temporal variation of the current in the ITER ELM control coils, while maintaining the relative toroidal phase of the currents in the three rows of ELM control coils constant (see figure 2) to ensure that the resulting resonant components of the RMP field applied remains as constant as possible through the temporal cycle [29]. The resulting heat and particle fluxes correspond to the toroidally averaged profiles obtained in the present simulations, i.e. the time averaged divertor power and particle fluxes at any toroidal location correspond to the toroidally averaged profiles over 1/3 of the toroidal length of the divertor target (n=3 symmetry is applied for the RMP field in our study). These toroidally averaged

divertor heat $q(s_{wall})$ and particle flux $\Gamma(s_{wall})$ profiles for the five magnetic topologies considered in the present study are shown in figure 9 at the OT and the IT of the ITER divertor. It is important to note that the particle flux profiles have been scaled by different factors so that they can be plotted in the same scale because of the impact of the particle balance boundary conditions chosen on divertor recycling as described in section 4. The modeling assumptions for the results in figure 9 are those in table 1 using n_{ISB} as boundary condition for the screened case, i.e. case no. 4 in table 1 is used for as screened case for this analysis. The lower part of figure 9 shows the toroidally averaged decay lengths of the divertor particle $\lambda_{\Gamma,t}$ and heat fluxes $\lambda_{q,t}$ at the inner and outer targets and their toroidally averaged peak values $\hat{\Gamma}$ and $\hat{q}$.

This toroidally averaged analysis points out that the peak heat flux is reduced to about 40% of the axisymmetric (no-RMP) peak flux value for the 15 MA plasma with $I_C = 90kAt$ in the vacuum approximation. The other cases have very similar toroidally averaged peak heat fluxes with a relatively small reduction of $9 - 14\%$ compared to the axisymmetric case. These values are similar to thos obtained directly from the toroidally asymmetric power fluxes in section 3 because the peak heat flux values correspond to those of the lobe close to the unperturbed separatrix, which is almost toroidally symmetric, as shown in figure 5.

In contrast, $\lambda_{q,t}$ and $\lambda_{\Gamma,t}$ at the divertor can be modified by the 3-D edge plasma transport. For the 15 MA plasma with $I_C = 90kAt$ in the vacuum approximation, $\lambda_{q,t}$ is approximately twice as large as that for the axisymmetric case leading to a wider average footprint for the divertor heat flux due to the 3-D RMP fields applied. For the case at $I_C = 45kAt$ and the one including screening, in fact, a reduction of $\lambda_{q,t}$ and $\lambda_{\Gamma,t}$ by 10% with plasma screening included and of up to 45% for the cases with $I_c = 45kAt$ are obtained. These modeling results shows that for these two perturbed magnetic topologies, even though the additional edge transport caused by the 3D fields is sufficient to decrease somewhat the value of the divertor peak heat flux, the additional parallel transport caused by 3D edge magnetic field structure in the lobes away from the separatrix leads to the concentration of the power fluxes along the target. This yields more peaked toroidally averaged divertor heat and particle deposition profiles than that caused by anomalous diffusion across the magnetic field in the SOL of the axisymmetric plasma which are broadened by the magnetic flux expansion at the divertor target. This finding might be an issue when the application of RMP fields for ELM control with divertor concepts such as the snowflake [81] or the super-X [82] divertor are considered, because these advanced divertor concepts rely on operation with very large flux expansion at the divertor targets.

6. Dependence of the 3-D heat and particle flux pattern on the perpendicular transport coefficients

In this section we explore the impact of the level of transport perpendicular to the magnetic field on the 3-D SOL transport features and on the divertor target heat and particle fluxes. The perpendicular transport level is provided as input to the modeling in the form of particle and heat diffusion coefficients $D_\perp$ and $\chi_\perp$. They are free modeling parameters, which in this study are set as fixed parameters in the entire radial modeling domain. Their values are taken based on experience with other models - for instance SOLPS for ITER case considered [34, 62].

For this assessment, we use the case at full RMP coil current and in the vacuum approximation (case No. 2 in table 1). We address two choices of anomalous transport coefficients; $D_\perp = 1/3$ $\chi_\perp = 0.4m^2/s$ (the same value as used in all cases discussed so far and shown in table 1) and a case with $D_\perp = 1/3$ $\chi_\perp = 0.8m^2/s$, i.e. an increase of the perpendicular transport coefficients by a factor of two. The modeling result is shown in figure 10 as 2-D maps of the divertor heat flux footprint and as 1-D divertor heat flux profiles along the divertor surface at toroidal angle $\phi = 0deg$. The increased perpendicular transport leads, as expected, to an increased widening of the heat flux pattern in the poloidal direction. However, we also see a significant elongation along the outwards direction of the helical finger structure, i.e. a longer decay length along the central line of the lobes at the divertor. This spreading of the heat fluxes causes a reduction of the peak heat flux densities clearly seen in the 2D profiles (figure 10.a-b) and, in a more quantitative way in the radial cut of $q_t(s_{wall})$ at $\phi = 0deg$ shown in figure 10(c). The peak heat fluxes in the three striated lobes are thus reduced from $8.1, 8.3, 6.3MW/m^2$ to $4.2, 5.7, 3.9MW/m^2$, respectively when the transport coefficients are increased.

An important outcome of these studies is that the shape of the heat flux profiles with RMP fields applied is modified in a very different way when the transport coefficients are varied with respect of the axisymmetric situation. In the axisymmetric situation an increase of the transport coefficients by a factor of 2 would lead to an increase of the heat flux decay length by a factor of $\sqrt{2}$ assuming a high recycling regime and a decrease of the peak heat flux by a factor of $\sqrt{2}$. In the case with 3-D fields modeled for ITER, the increase of the anomalous transport coefficients leads to a change in the sharing of the heat flux between the lobes and to a higher peak heat flux in the second lobe, further away from the separatrix, than in the first one near the separatrix. This is the result of the fact that numerous open short connection length field lines are present in the plasma periphery [12, 29] as a consequence of the strong edge stochastization with $I_c = 90kAt$ in the vacuum field assumption. In these circumstances the increased radial transport leads to significant flux of plasma energy and particles into the second and the further outwards lobes resulting in a higher power flux at the position of these outward

lobes than into the first lobe closer to the separatrix. For more detailed studies of the edge magnetic field line topology following the application of 3-D resonant fields the reader is referred to [27] and [59]. Although both studies were carried out for DIII-D, the discharges considered for DIII-D have ITER similar plasma shape, safety factor q_{95} and magnetic shear so that the results of that study are relevant to ITER matter of the required rescaling to take into account the different plasma dimensions.

7. Impact of RMP coil failure on toroidal heat flux pattern

The ITER ELM control coil set is designed to have redundancy so that it can meet its design criterion in case of the failure of a small number of ELM control coils. This is discussed in detail in [2, 29]. To address the impact of such a coil malfunction on the divertor flux results discussed so far, we address here a worst case in which three ELM control coils are not functional in the standard Q=10 H-mode scenario for ITER and based on the $I_c = 90kAt$ reference coil current case in the vacuum approximation. The three failing coils are aligned to the edge magnetic field line pitch angle, as shown in 11.a to induce the strongest distortion of the optimized resonant field amplitudes in this RMP setup [29]. We thus consider a case in which the current in the coils highlighted in red in figure 11.a is set to zero while the amplitude and phase of the current in the other coils is adapted to recover some part of the spectral components lost due to the absence of current in these three coils. The vacuum island overlap was used as figure of merit in the accompanying study [29] to assess how far ELM control could be recovered based on this criterion. The values of the re-optimized currents are included in figure 11.a in $[kAt]$. For reference, the level of vacuum island overlap obtained with this re-optimization is the same as that for the full set of ELM control coils operated with $I_C = 45kAt$ (case No. 4 in table 1) and the heat flux results obtained should thus be compared with those for this case.

The resulting 2-D divertor heat fluxes along the entire 360 degree toroidal angle at the IT and the OT for the ELM control coil configuration and currents in figure 11.a are shown in figure 11.b. So far, the $n = 3$ symmetry in the RMP field applied was used to reduce the modeling domain to $120deg$ toroidally. However, in order to assess asymmetries born from non-harmonic perturbations do to the three malfunctioning coils, we need to assess the full $360deg$ divertor flux pattern. Such asymmetries, for example one of the helical lobes at the divertor being significantly shorter that the other two, can result in different requirements for the rotation of the heat flux pattern to avoid thermal fatigue of the ITER divertor target [2].

Our calculations in figure 11 b-c show, however, that the n=3 toroidal symmetry of the heat fluxes at the divertor remains practically unaffected. They are very similar to the result with all ELM control coils operating at $I_c = 45kAt$ and using the vacuum field approximation (case No. 4 in table 1 and figure 5). Some effects are nevertheless

seen particularly at the inner divertor. Here, a more extended heat flux along the lobe reaching the divertor at 360 deg than at 240 deg and 120 deg is found, but the level of this asymmetry is small. Consistent with this, we find that the effect of the 3-D resonant perturbation with three failed coils on the thermal and particle confinement of the confined plasma is similar to those of Case No. 4 in table 1. Indeed applying the re-optimization method described in [29], it is possible to maintain the same level of vacuum island overlap and a very similar 3-D edge magnetic configuration for the worst case with failure in three field-aligned ELM control coils compared to the case in which all 27 ITER ELM control coils are utilized.

8. Discussion, Conclusion and Outlook

The results of 3D fluid plasma and kinetic neutral transport modeling with EMC3-EIRENE presented in this paper show that during application of RMP fields for ELM control at ITER, a toroidally asymmetric pattern of the divertor heat and particle fluxes will be produced. The features of this pattern depend on the level of current in the ELM control coils I_C and on the plasma response to the edge magnetic perturbation applied. For typical conditions in the ITER 15 MA Q = 10 scenario and the highest level of $I_c = 90kAt$ without plasma response effects, the area over which heat and particles is deposited at the divertor are much larger then in the axisymmetric case. This significantly decreases the peak heat flux values on the divertor but, however, still significant heat fluxes in the order of $2 - 5MWm^{-2}$ can occur to areas at the outer divertor target which are strongly shaped and where such heat flux levels would be problematic [Pitts2011]. This spreading and the reduction of the associated divertor fluxes is more moderate for cases with lower $I_c = 45kAt$ using the vacuum field approximation and when a strongly screening plasma response is included. In all of the cases studied (with attached divertor conditions and moderate ionization energy losses) the resulting maximum peak and particle fluxes when 3-D fields are applied are equal or lower to those corresponding to the axisymmetric situation (without RMP fields) with the same modeling assumptions.

The RMP fields have in addition a strong impact on the energy and particle confinement of the main plasma. For the highest I_C values and without a plasma response, the modeled effect on the thermal confinement of the ITER 15 MA Q = 10 scenario is significant. The temperature at the inner simulation boundary is reduced by a factor of two. This strong decrease of global energy confinement is reduced when a strongly screening plasma response is considered as well as when I_C is reduced to $45kAt$. The thermal confinement loss is limited to below 20% and hence to a level more similar to that seen in experiments (decrease of energy confinement by $\approx 10\%$.).

The application of 3-D fields also has a significant effect on the particle confinement. With full $I_C = 90kAt$, a reduction of the particle confinement time τ_P of $\Delta\tau_P \approx 35\%$

compared to the axisymmetric case is found. This is due to the formation of a checkerboard pattern of SOL like plasma flow channels which connect the confined plasma with the PFCs allowing plasma particles to directly flow out of the confined plasma. These flow channels affect the net particle flow out of the confined plasma and the magnitude of the divertor particle fluxes that are achieved for a given level of edge plasma density, i.e. the divertor recycling regime. At the ams time, these flow channels can also alter the edge momentum flux due to the counter streaming flows, which is found to affect the efficiency of the fueling by recycling neutrals and could affect plasma detachment behaviour [57, 75]. It is important to note that these helical SOL bundles also persist at lower I_C and even with strong screening included. A still significant reduction of $\Delta\tau_P \approx 15 - 20\%$ is therefore found in the modeling result for these cases. Because of the difficulty measuring the total wall recycling flux in nowadays toroidal devices, no full experimental particle balance assessment and no direct measurements of τ_P with RMP fields are available. Therefore, a quantitative comparison of the modeling results with experiments concerning the impact on the particle confinement is not possible. This is a significant gap since the results presented here indicate that significantly increased fueling might be necessary to recover the density required for a fusion gain of $Q = 10$. A detailed assessment in comparison with nowadays experiments is important as this result directly affects the demands on the ITER pellet fueling capacity as well as the issue of compatibility with the Tritium throughput allowance.

Analysis of the toroidally averaged heat and particle flux profiles shows that the shape of the toroidally averaged divertor target flux profiles is defined by the specific shape of the helical magnetic footprint induced by the RMP fields. Thus, the toroidally averaged heat flux patterns are wider than in the axisymmetric situation for the case at $I_c = 90kAt$ and without plasma response. On the contrary they are narrower when the strongly screening plasma response is included. In the latter case the channelling of the heat flux from the core plasma into the helical structures created by the RMPs leads to a faster decrease of the toroidally averaged heat flux profiles away from the separatrix than in the axisymmetric situation. In the latter, the effective divertor area for power deposition is determined by energy diffusion across the 2D magnetic surfaces and parallel transport along the field lines. The modeling indicates that the 3-D helical SOL structure induced by the RMP fields might actually counteract the natural spreading achieved by magnetic flux expansion in the axisymmetric case. Increasing the radial transport coefficients yields an enhanced filling of the helical divertor lobes with RMP fields applied. This represents a quite different mechanism compared to the axisymmetric case. Without RMP fields, the two fold enhanced perpendicular heat and particle diffusion levels addressed in this study yield a $\sqrt{2}$ increase of the divertor flux decay length and of the peak flux levels. In contrast, with an applied RMP fiel, a strong influx into the helical lobe pattern results in a localized increase of the heat and particle fluxes at the positions of the helical lobe footprint. Hence, the impact of increased perpendicular particle and energy fluxes on the wetted area on the divertor

can be significantly larger when RMP fields are applied.

A critical gap in the analysis presented is modeling of a dissipative, i.e. detached and highly radiative divertor solution including direct compareison to suitable experimental data. This also involves the necessity of demonstrating ELM suppression combined with a detached divertor and use of active control means like gas injection to maintain such a highly dissipative divertor. Modeling of this regime leads to numerical instabilities when EMC3-EIRENE is used for the tokamak situation due to the scaled nature of the particle balance. However, high density, radiative divertor operation is required for the control of divertor power fluxes at ITER [34, 35]. Therefore, understanding the effect of RMP fields on this divertor regime is very important, as the use of RMP fields for ELM control in ITER must be compatible with the requirements for stationary power load control. In order to address this, a number of improvements are currently being included in the code to allow progress in the simulation of more realistic dissipative divertor solutions. These efforts include:

- improvement of EMC3-EIRENE stability for low divertor temperatures/high divertor densities (first results reported in [68])
- generalization of the particle balance in EMC3-EIRENE to enable inclusion of volumetric particle sources and sinks as required for the modeling of divertor detachment
- inclusion of a more realistic description of impurity transport in the EMC3 domain [56]

An additional and very important outstanding issue concerns the modeling of the erosion/deposition balance in a radiative divertor when 3-D fields are applied. The 3-D plasma edge structure and, in particular, the helical flow channels that it induces [40] can potentially significantly affect the resulting erosion deposition balance on the divertor targets and the main wall. On-going studies address these issues through an improved description of the toroidally asymmetric 2-D impurity source with TRIM data for physical sputtering in EIRENE and then assess the erosion and deposition features on the 3-D EM3C-EIRENE background plasma using ERO [83, 84] or the Monte Carlo Impurity model MCI [85].

The first systematic assessment of 3-D edge transport and divertor particle and heat fluxes during the application of RMP fields for ELM control in ITER presented in this paper has highlighted their strong sensitivity to the real 3-D magnetic field topology of the plasma. Besides the expected strong relation between the resulting field stochasticity and thermal confinement, the generation of helical parallel plasma flow channels has been demonstrated. Since these 3-D transport features depend very sensitively on the actual resonant field amplitudes in the plasma and on the effective radial magnetic field structure perturbing the separatrix, obtaining reliable predictions for the plasma response at ITER is urgent. This is highlighted by the fact that recent experimen-

tal results consistently show that a dominant kink-mode plasma response amplifies the local resonant field amplitudes in the region of the pedestal top, which increases the radial field components perturbing the separatrix. This amplifying response seems to be mixed into a general screening response on rational surfaces with sufficient diamagnetic electron flow. Therefore, the strongly screening plasma response used in this study is only one possible plasma response solution and the real resultant 3-D boundary shape could be more similar to the vacuum field approximation. Combination of advanced plasma response modeling in full toroidal geometry with EMC3-EIRENE to obtain a self-consistent SOL modeling result during RMP ELM control at ITER is an important next step. The study presented here highlights that the development of the EMC3-EIRENE code for modeling of detached plasma scenarios should be accompanied by progress in understanding and modeling of the plasma response to 3-D fields [36]. A reliable extrapolation of plasma response effects to ITER is needed in order to specify a 3-D magnetic topology which is produced in the plasma. This, alongside at least the highlighted improvements to EMC3-EIRENE, is essential to obtain a solid physics-based evaluation of the effect of RMP fields applied for ELM control in the ITER radiative divertor conditions and the associated erosion/deposition balance.

Disclaimer The views and opinions herein do not necessarily reflect those of Fusion for Energy (F4E) or those of the ITER Organization.

Acknowldgements This work was supported by ITER task IO/CT/11/4300000497, Fusion for Energy (F4E) grant GRT-055(PMS-PE), Startup Funds of the Department of Engineering Physics and the College of Engineering at the University of Wisconsin - Madison and by the Department of Energy under grant DE-SC0013911. Generous provision of computing resources by the John von Neuman Institute for Computing (NIC) at the Juelich Supercomuting Centre (JSC), Germany is gratefully acknowledged. Modeling was done on the JUROPA super-computer operated by JSC and the Fusion-HPC super-computer funded by the European Fusion Development Agreements (previously EFDA, now EUROFUSION).

9. Figures

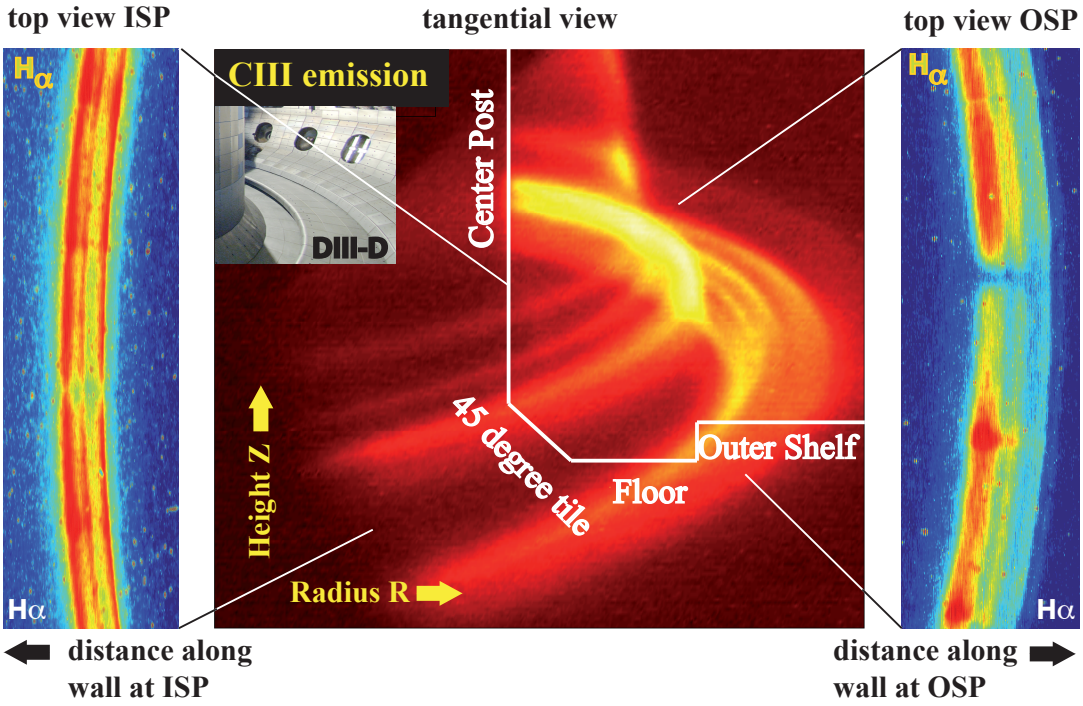

Figure 1: Divertor light emission patterns showing the formation of a three-dimensional plasma boundary during suppression of edge localized modes by resonant magnetic perturbations fields at DIII-D. A tangential view in the light of double-ionized carbon is shown in the middle figure. The left and right figures show the Balmer-alpha emission of deuterium at the inner (ISP, left side) and the outer (OSP, right side) divertors.

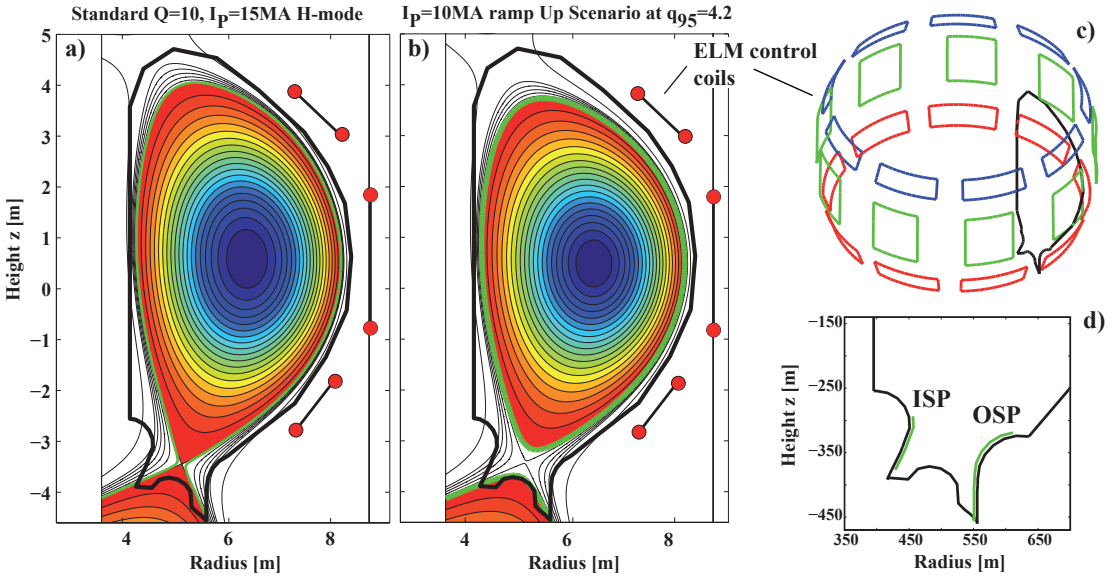

Figure 2: ITER plasma equilibria used in this study (figure a, b), layout of the ITER ELM control coil set (figure c) and ITER divertor geometry with the inner and outer divertor strike zones areas analyzed in these studies (figure d).

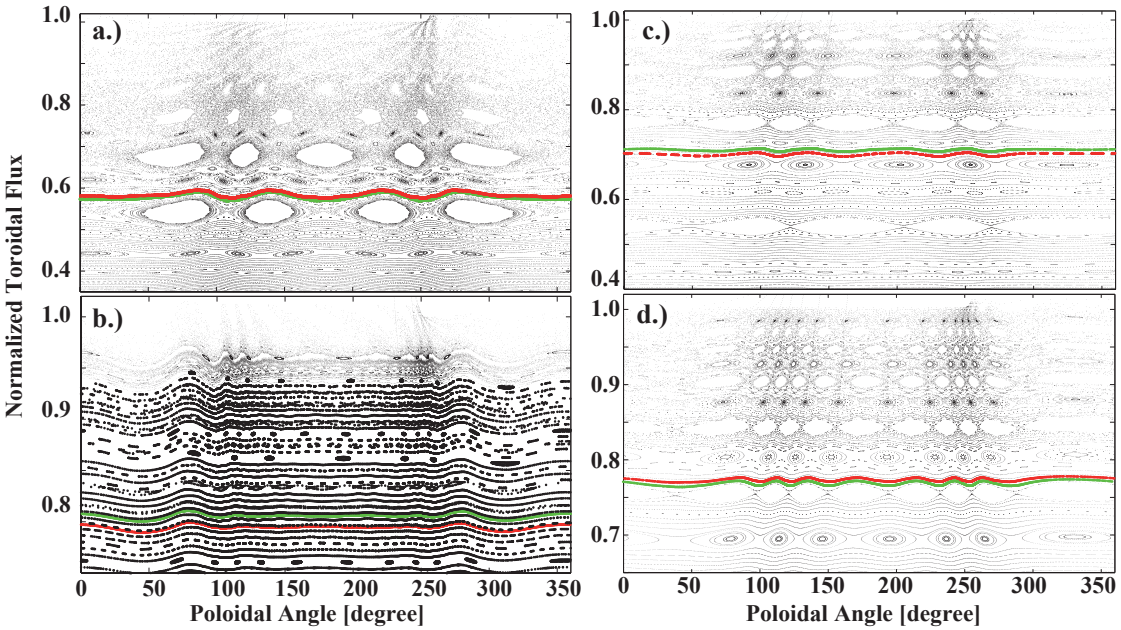

Figure 3: ITER perturbed magnetic field topologies considered visualized as Poincare plots from field line tracing. The effect of the linear reduction of the ELM control coil current is shown in figure a (90kAt in vacuum) to figure c (45kAt in vacuum) for the 15 MA Q=10 plasma. The effect of plasma response shielding all resonant modes with $n = 3, 6$ and $m < 8$ and allowing vacuum like penetration for all modes with $m > 7$ on magnetic field topology for 15 MA Q = 10 plasmas with 90 kAt is illustrated in figure a (to be compared with figure a for the vacuum case). The effect of increased edge shear at high $q_{95} = 4.2$ and with 45kAt in the vacuum approximation on the edge magnetic field topology is illustrated in in figure d. The two flux surfaces used as inner simulation boundary for all cases are depicted as red and green colored field line traces.

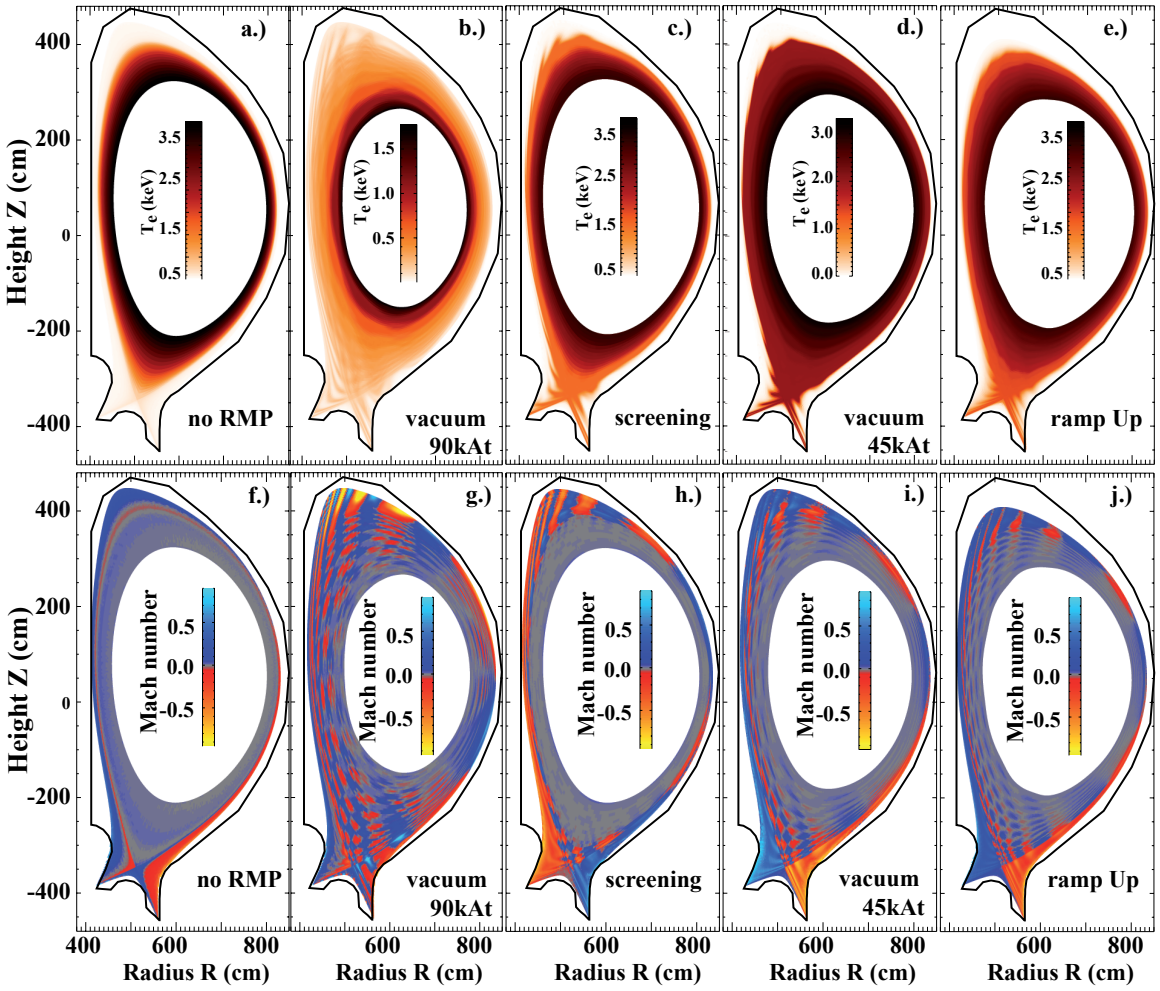

Figure 4: Electron temperature (upper row, figure a-e) and Mach number of the plasma parallel flow (lower row, figures f-j) for the 3-D magnetic field topologies studied. The formation of a three-dimensional, helical scrape off layer is seen with high temperature plasma fingers reaching the divertor targets target. The extension of these fingers depends on the resonant field amplitude at the separatrix (including plasma response effects) and the temperature of the plasma in the stochastized edge layer. The helical fingers lead to a direct connection between the plasma inside the 2-D plasma separatrix and the plasma facing components which creates plasma power and particle flows from the confined plasma to the plasma facing components.

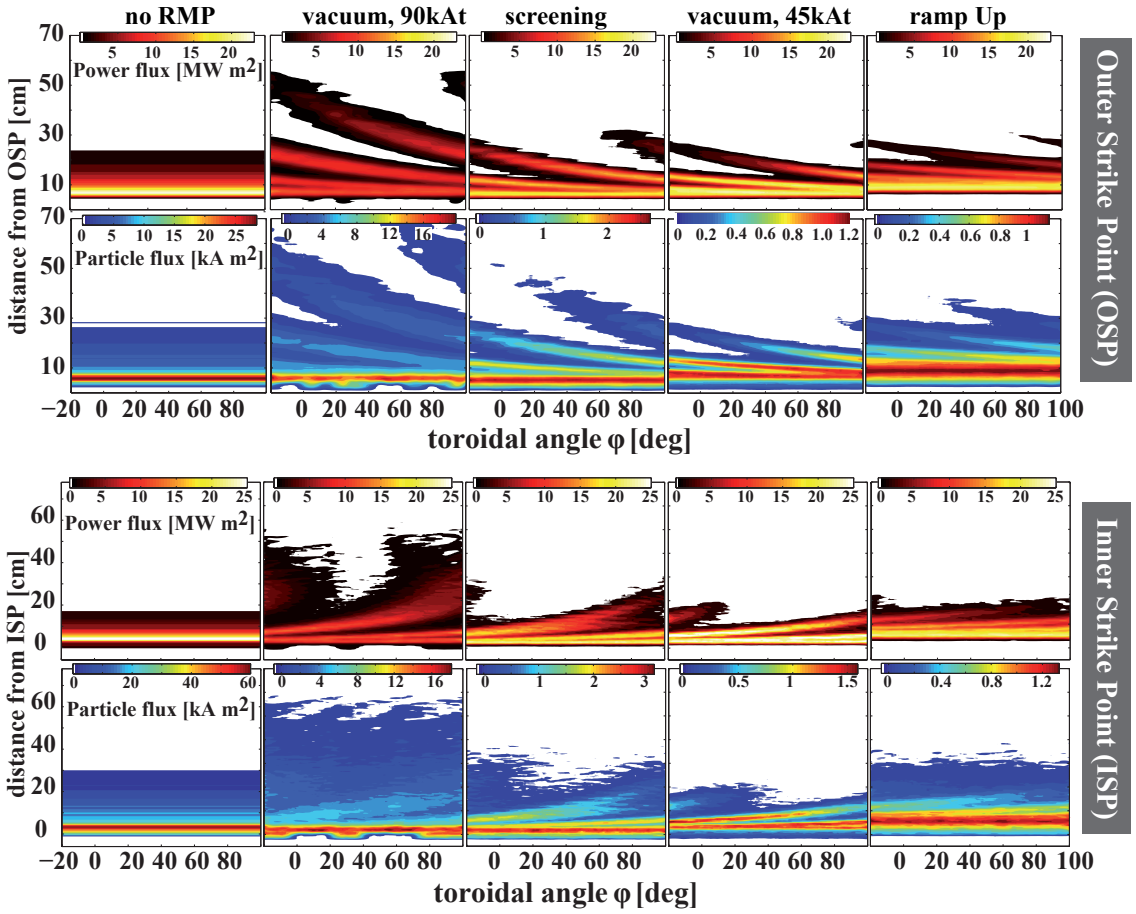

Figure 5: Divertor heat and particle flux distributions at the outer (upper block) and inner (lower block) divertor targets for the four 3-D magnetic topologies studied and the axisymmetric (no RMP) reference case. In each of the two blocks, the upper row of figures corresponds to the heat flux and the lower row the particle flux to the divertor target. A pronounced striation of both heat and particle fluxes is seen at both divertor targets. The helical extension of these lobes is determined by the effective resonant field amplitudes at the separatrix and the actual level of the fluxes that reach these upstream location which are a result of the the stochastization of the plasma inside the separatrix by the applied fields.

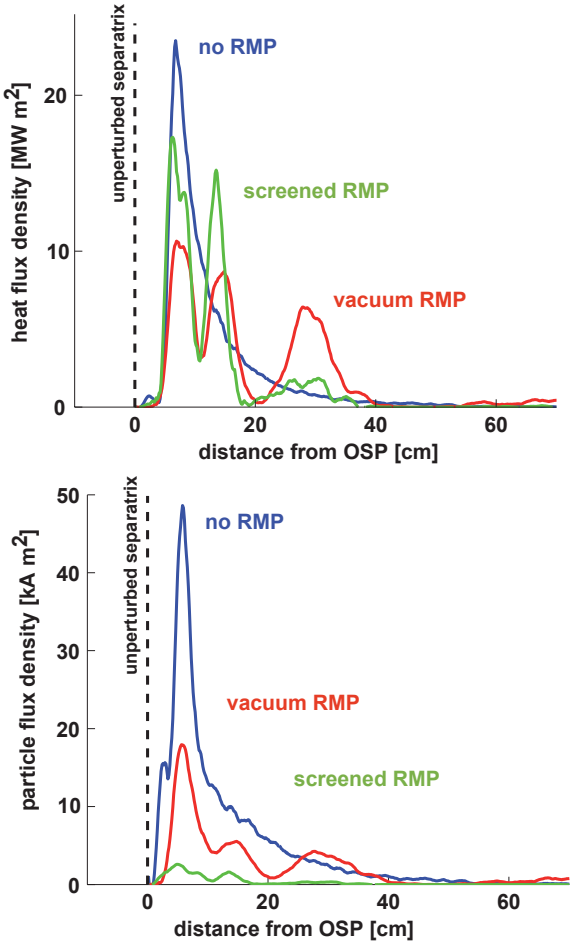

Figure 6: Heat and particle flux density profiles for 15 MA Q=10 plasmas. This figure shows the reference axisymmetric case (noRMP -blue profile), the case with 90 kAt in the ELM control coils and the edge magnetic field in the vacuum approximation (vacuum RMP-red profile) and including plasma screening (screened RMP - green profile) at toroidal angle of $\phi = 0deg$. A pronounced reduction of the peak heat flux and associated broadening of the heat flux profile is seen for the vacuum RMP case. The changes to the heat flux for the screened-RMP case are much smaller and lead to toroidally averaged profiles for the screened RMP case which are comparable to the axisymmetric case as shown in figure 7. The strong reduction of the particle flux density when 3-D fields are applied is associated with the effect of the 3-D fields on the particle balance resulting from the modeling assumptions in the EMC3-Eirene code version used.

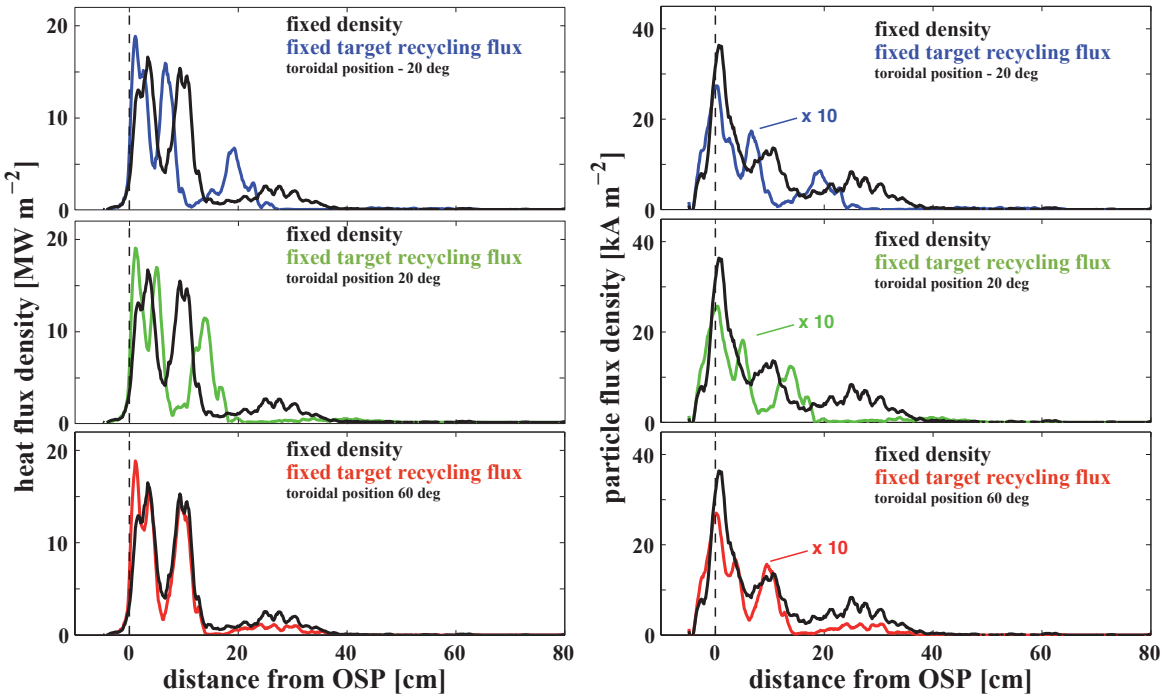

Figure 7: Divertor heat (left)) and particle (right) flux density profiles at $\phi = -20, 20, 60 deg$ for two ITER 15 MA Q=10 cases with $I_C = 90 kAt$ including plasma response. Colored profiles are shown for modeling in which the target recycling flux was used as boundary condition and black profiles show results in which the upstream density at the inner simulation boundary was used as boundary conditions. The use of target recycling as boundary condition leads to much larger (by a factor of 10) particle fluxes at the divertor than the case in which the plasma density is used as boundary condition. Despite this large difference in particle fluxes the peak heat fluxes and total power fluxes to the divertor are similar for the two cases, as divertor is attached and the ionization losses remain low in both cases. A visible effect of the recycling flux on the heat flux profiles is the change of position of the peaks in these profiles associated with the intersections of the lobes with the divertor targets.

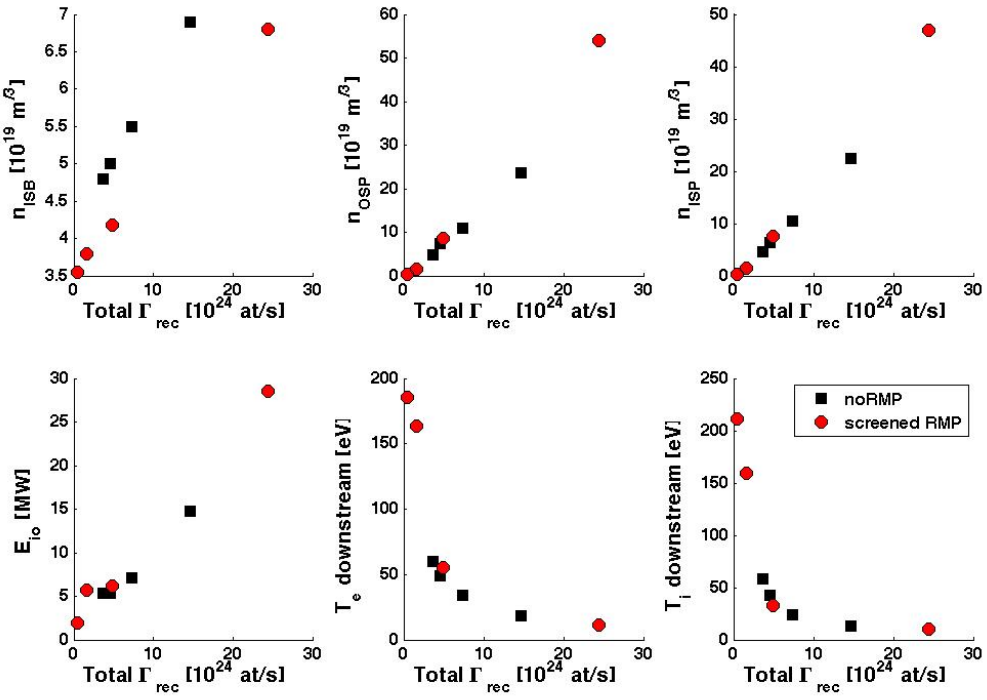

Figure 8: Upstream (inner simulation boundary (ISB) and inner (ISP) and outer (OSP) divertor plasma density and temperature and total ionization losses versus total recycling losses for a recycling scan study. The axisymmetric case is compared to a case with ELM control coils with $I_c = 90kAt$ including plasma screening for ITER 15 MA Q=10 plasma conditions. The reduction of the particle confinement by the application of 3-D resonant fields is identified by the fact that a substantially increased recycling source is needed to achieve the same density at the inner simulation boundary when screened 3-D fields are applied compared to the axisymmetric case. The achieved divertor density and temperature range shows that for both cases with screened 3-D fields and without them a high density, low temperature divertor can be obtained corresponding to a high recycling regime. The detailed results discussed in the paper correspond to the highest density/recycling flux in these simulations.

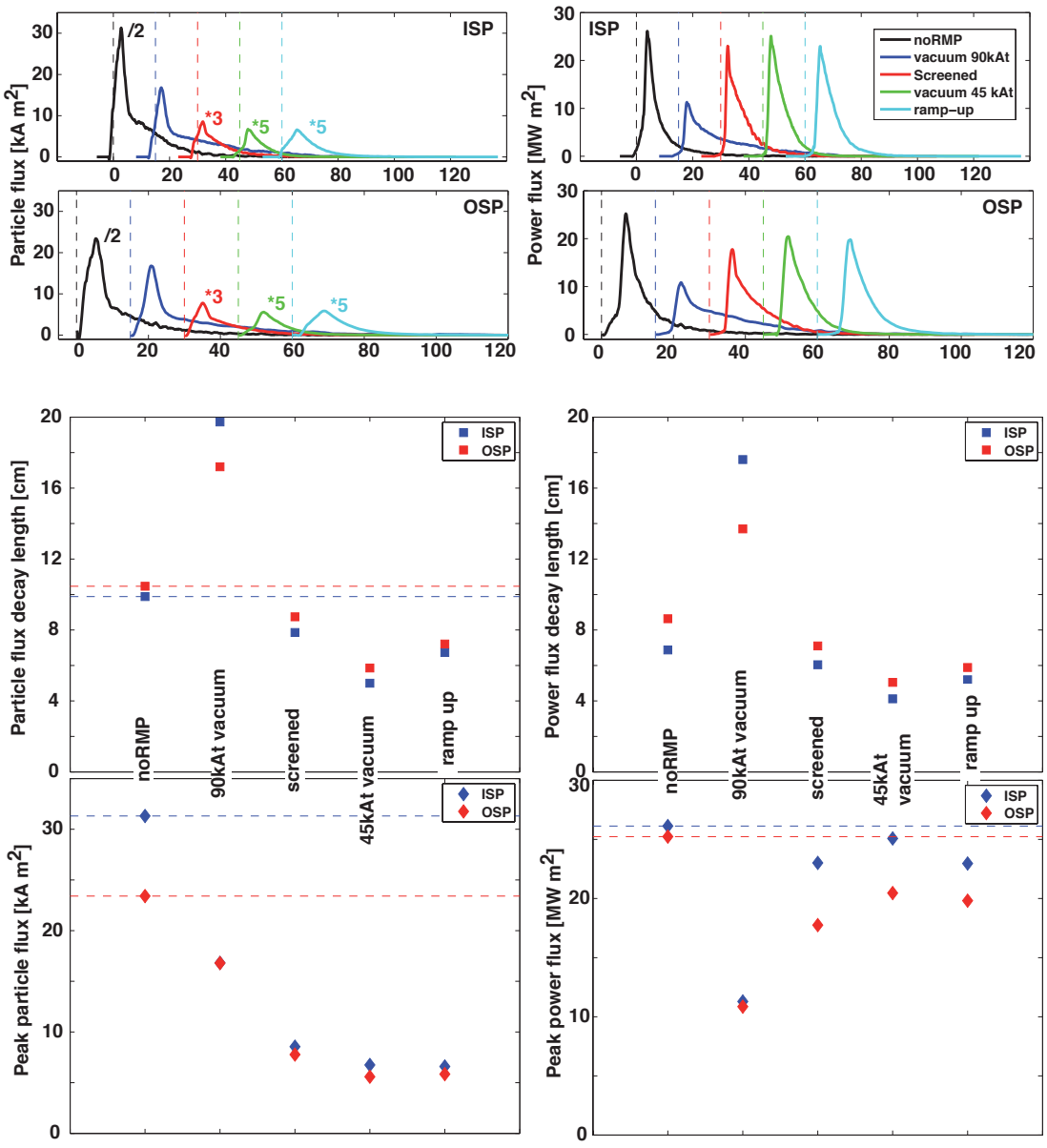

Figure 9: Toroidally averaged heat and particle flux density profiles for the five magnetic topologies studied. A significant reduction of the peak heat flux and widening of the heat flux profiles is only observed with the 3-D field case with ELM coil current $I_c = 90kAt$ in the vacuum approximation. For all the other cases the reduction of peak heat flux profiles is negligible and together with it the heat flux profile does not change significantly. For some cases with 3-D fields the heat flux profiles can actually be narrower than in the axisymmetric case due the effective channeling of the heat flux into the perturbed separatrix topology which can overcompensate the heat flux spreading effect of diffusion across the field and the magnetic flux expansion at the divertor in the axisymmetric case.

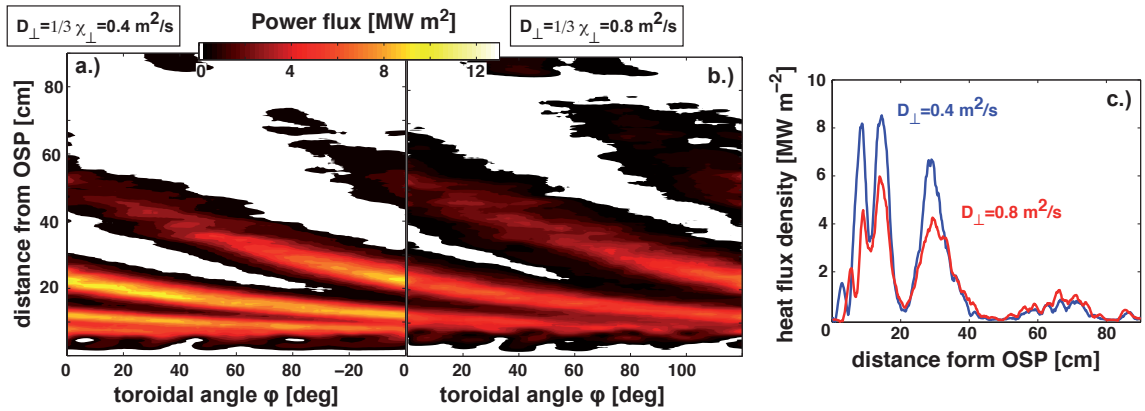

Figure 10: 2D distributions of heat flux density for the 15 MA Q=10 case with $I_c = 90kAt$ in the vacuum approximation and two levels of perpendicular transport coefficients (figures a and b). Figure c shows the heat flux density profiles taken at $\phi = 0deg$). Increasing perpendicular transport coefficients results in a spreading of the heat fluxes radial outwards into the helical lobe pattern modifying the relative magnitude of the peak heat fluxes in the lobes at various distances to the separatrix strike point.

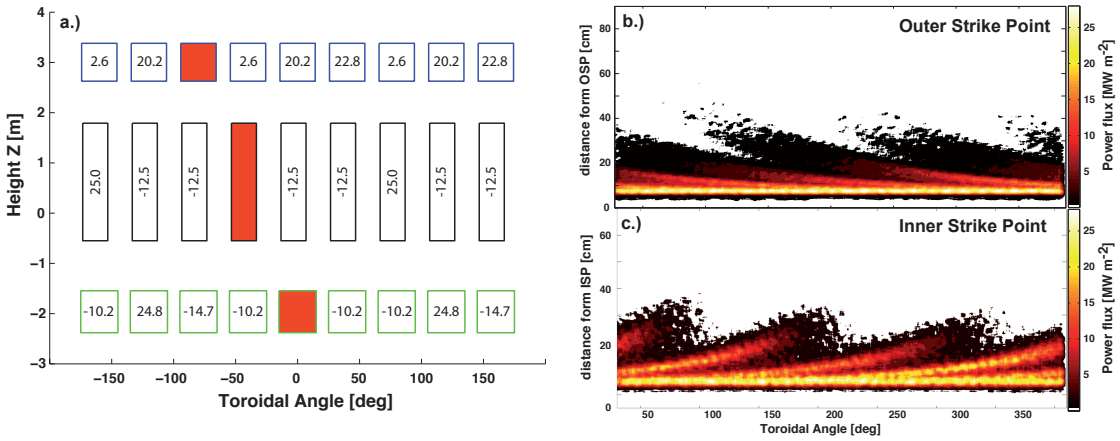

Figure 11: Divertor heat flux density profiles for a case corresponding to failure in three field aligned ELM control coils (i.e. the worst three ELM control coil failure scenario). Figure a illustrates the layout of the unavailable three ELM control coils and the currents used in the remaining 24 coils. The full $360deg$ distribution of the divertor target heat flux density at the outer and inner divertor targets are shown in figures b-c respectively. Figures b-c show that the heat flux density profiles when three ELM control coils are not utilized lose the perfect $120deg$ symmetry obtained when all the 27 coils are operating. However, the differences of the heat flux density profiles with respect to this perfect $120deg$ symmetry situation are small, as shown by the toroidal cuts of the profiles in figures b-c at $phi = 120, 240$ and $360deg$ in figure d for the outer divertor target.

[1] A. Loarte, D.J. Campbell, Y. Gribov, R.A. Pitts, N. Klimov, V. Podkovyrov, A. Zhitlukhin, I. Landman, S. Pestchanyi, B. Bazylev, J. Linke, T. Loewenhoff, G. Pintsuk, O. Schmitz, Y. Liang, T.E. Evans, M. Schaffer, M.E. Fenstermacher, M. Becoulet, G. Huysmans, E. Nardon, L. Baylor, J. Canik, R. Maingi, J.W. Ahn, B. Riccardi, G. Saibene, R. Sartori, M. Cavinato, T. Eich, M. Jakubowski, P.T. Lang, H. Thomsen, W. Suttrop, E. De la Luna, H. Wilson, and A. Kirk. ITER ELM control requirements, ELM control schemes and required R&D. In *Proceedings of the IAEA Fusion Energy Conference 2010, ITR/1-4*, 2010.

[2] A. Loarte, G. Huijsmans, S. Futatani, L.R. Baylor, T.E. Evans, D. M. Orlov, O. Schmitz, M. Becoulet, P. Cahyna, Y. Gribov, A. Kavin, A. Sashala Naik, D.J. Campbell, T. Casper, E. Daly, H. Frerichs, A. Kischner, R. Laengner, S. Lisgo, R.A. Pitts, G. Saibene, and A. Wingen. Progress on the application of elm control schemes to iter scenarios from the non-active phase to dt operation. *Nuclear Fusion*, 54(3):033007, 2014.

[3] T.E. Evans, D. Orlov, A. Wingen, W. Wu, A. Loarte, T. Casper, O. Schmitz, G. Saibene, and M. J. Schaffer. 3D vacuum field modeling of the ITER ELM control coils during standard operating scenarios. 2012. Synopsis, to be presented at IAEA Fusion Energy Conference 2012, San Diego, CA, USA.

[4] T.E. Evans. ELM mitigation techniques. *Journal of Nuclear Materials*, 438(0):S11 – S18, 2013.

[5] T. E. Evans, R. A. Moyer, P. R. Thomas, J. G. Watkins, T. H. Osborne, J. A. Boedo, E. J. Doyle, M. E. Fenstermacher, K. H. Finken, R. J. Groebner, M. Groth, J. H. Harris, R. J. La Haye, C. J. Lasnier, S. Masuzaki, N. Ohyabu, D. G. Pretty, T. L. Rhodes, H. Reimerdes, D. L. Rudakov, M. J. Schaffer, G. Wang, and L. Zeng. Suppression of large edge-localized modes in high-confinement DIII-D plasmas with a stochastic magnetic boundary. *Phys. Rev. Lett.*, 92:235003, Jun 2004.

[6] T.E. Evans, M.E. Fenstermacher, R.A. Moyer, T.H. Osborne, J.G. Watkins, P. Gohil, I. Joseph, M.J. Schaffer, L.R. Baylor, M. Becoulet, J.A. Boedo, K.H. Burrell, J.S. deGrassie, K.H. Finken, T. Jernigan, M.W. Jakubowski, C.J. Lasnier, M. Lehnen, A.W. Leonard, J. Lonnroth, E. Nardon, V. Parail, O. Schmitz, B. Unterberg, and W.P. West. RMP ELM suppression in DIII-D plasmas with ITER similar shapes and collisionalities. *Nuclear Fusion*, 48(2):024002, 2008.

[7] O. Schmitz, T.E. Evans, M.E. Fenstermacher, A. McLean, J. Boedo, N.H. Brooks, H. Frerichs, M. Jakubowski, R. Laengner, C.L. Lasnier, A. Loarte, R.A. Moyer, D. Orlov, H. Reimerdes, D. Reiter, U. Samm, H. Stoschus, E.A. Unterberg, and J.G. Watkins. The influence of three-dimensional stochastic magnetic boundaries on plasma edge transport and the resulting plasma wall interaction. *Journal of Nuclear Materials*, 415(1, Supplement):S886 – S893, 2011.

[8] O Schmitz, T E Evans, M E Fenstermacher, H Frerichs, M W Jakubowski, M J Schaffer, A Wingen, W P West, N H Brooks, K H Burrell, J S deGrassie, Y Feng, K H Finken, P Gohil, M Groth, I Joseph, C J Lasnier, M Lehnen, A W Leonard, S Mordijck, R A Moyer, A Nicolai, T H Osborne, D Reiter, U Samm, K H Spatschek, H Stoschus, B Unterberg, E A Unterberg, J G Watkins, R Wolf, the DIII-D, and TEXTOR Teams. Aspects of three dimensional transport for ELM control experiments in ITER-similar shape plasmas at low collisionality in DIII-D. *Plasma Physics and Controlled Fusion*, 50(12):124029, 2008.

[9] O. Schmitz, T.E. Evans, M.E. Fenstermacher, M.J. Lanctot, C.L. Lasnier, S. Mordijck, R.A. Moyer, H. Reimerdes, and the DIII-D Team. Formation of a three-dimensional plasma boundary after decay of the plasma response to resonant magnetic perturbation fields. *Nuclear Fusion*, 54(1):012001, 2014.

[10] R.J. Buttery, T.C. Hender, J.D. Ashall, K.B. Axon, G. Blow, and S.J. Fielding. Effects of resonant magnetic perturbations on divertor target power loads in COMPASS-D. *Nuclear Fusion*, 36(10):1369, 1996.

[11] M.W. Jakubowski, S.S. Abdullaev, K.H. Finken, and the TEXTOR Team. Modelling of the magnetic field structures and first measurements of heat fluxes for TEXTOR-DED operation. *Nuclear Fusion*, 44(6):S1, 2004.

[12] O. Schmitz, M.W. Jakubowski, H. Frerichs, D. Harting, M. Lehnen, B. Unterberg, S.S. Abduallaev, S. Brezinsek, I. Classen, T. Evans, Y. Feng, K.H. Finken, M. Kantor, D. Reiter, U. Samm, B. Schweer, G. Sergienko, G.W. Spakman, M. Tokar, E. Uzgel, R.C. Wolf, and the TEXTOR Team. Identification and analysis of transport domains in the stochastic boundary of TEXTOR-DED for different mode spectra. *Nuclear Fusion*, 48(2):024009, 2008.

[13] J.-W. Ahn, J.M. Canik, V.A. Soukhanovskii, R. Maingi, and D.J. Battaglia. Modification of divertor heat and particle flux profiles with applied 3d fields in nstx h-mode plasmas. *Nuclear Fusion*, 50(4):045010, 2010.

[14] P. Cahyna and E. Nardon. Model for screening of resonant magnetic perturbations by plasma in a realistic tokamak geometry and its impact on divertor strike points. *Journal of Nuclear Materials*, 415(1, Supplement):S927 – S931, 2011.

[15] H.W. Mueller, T. Lunt, W. Suttrop, T. Eich, R. Fischer, J.C. Fuchs, A. Herrmann, M. Kofcan, P. de Marnoe, and E. Wolfrum. Modification of scrape-off layer transport and turbulence by non-axisymmetric magnetic perturbations in ASDEX upgrade. *Journal of Nuclear Materials*, 438, Supplement(0):S64 – S71, 2013.

[16] A Kirk, I T Chapman, T E Evans, C Ham, J R Harrison, G Huijsmans, Y Liang, Y Q Liu, A Loarte, W Suttrop, and A J Thornton. Understanding the effect resonant magnetic perturbations have on elms. *Plasma Physics and Controlled Fusion*, 55(12):124003, 2013.

[17] M. E. Fenstermacher, W. H. Meyer, R. D. Wood, D. G. Nilson, R. Ellis, and N. H. Brooks. A tangentially viewing visible tv system for the diii-d divertor. *Review of Scientific Instruments*, 68(1):974–977, 1997.

[18] T E Evans, R K W Roeder, J A Carter, B I Rapoport, M E Fenstermacher, and C J Lasnier. Experimental signatures of homoclinic tangles in poloidally diverted tokamaks. *Journal of Physics: Conference Series*, 7(1):174, 2005.

[19] M.W. Jakubowski, T.E. Evans, M.E. Fenstermacher, M. Groth, C.J. Lasnier, A.W. Leonard, O. Schmitz, J.G. Watkins, T. Eich, W. Fundamenski, R.A. Moyer, R.C. Wolf, L.B. Baylor, J.A. Boedo, K.H. Burrell, H. Frerichs, J.S. deGrassie, P. Gohil, I. Joseph, S. Mordijck, M. Lehnen, C.C. Petty, R.I. Pinsker, D. Reiter, T.L. Rhodes, U. Samm, M.J. Schaffer, P.B. Snyder, H. Stoschus, T. Osborne, B. Unterberg, E. Unterberg, and W.P. West. Overview of the results on divertor heat loads in RMP controlled H-mode plasmas on DIII-D. *Nuclear Fusion*, 49(9):095013, 2009.

[20] A. Wingen, O. Schmitz, T. E. Evans, and K. H. Spatschek. Heat flux modeling using ion drift effects in diii-d h-mode plasmas with resonant magnetic perturbations. *Physics of Plasmas (1994-present)*, 21(1):012509, 2014.

[21] M.W. Shafer, E.A. Unterberg, D.M. Orlov, T.E. Evans, J.H. Harris, D.L. Hillis, R. Maingi, R.A. Moyer, R. Nazikian, and A. Wingen. Experimental imaging of separatrix splitting on diii-d. *Nuclear Fusion*, 52(12):122001, 2012.

[22] S. S. Abdullaev, M. Jakubowski, M. Lehnen, O. Schmitz, and B. Unterberg. On description of magnetic stochasticity in poloidal divertor tokamaks. *Physics of Plasmas*, 15(4):042508, 2008.

[23] T. Kroetz, M. Roberto, I.L. Caldas, R.L. Viana, P.J. Morrison, and P. Abbamonte. Integrable maps with non-trivial topology: application to divertor configurations. *Nuclear Fusion*, 50(3):034003, 2010.

[24] A. Punjabi, H. Ali, and A. Boozer. Effects of dipole perturbation on the stochastic layer and magnetic footprint in single-null divertor tokamaks. *Physics of Plasmas*, 10(10):3992–4003, 2003.

[25] T. E. Evans, R. K. W. Roeder, J. A. Carter, and B. I. Rapoport. Homoclinic tangles, bifurcations and edge stochasticity in diverted tokamaks. *Contributions to Plasma Physics*, 44(1-3):235–240, 2004.

[26] R K W Roeder, B I Rapoport, and T E Evans. Explicit calculations of homoclinic tangles in tokamaks. *Phycsis of Plasmas*, 10(9):3796–3800, 2003.

[27] A. Wingen, T.E. Evans, and K.H. Spatschek. High resolution numerical studies of separatrix

splitting due to non-axisymmetric perturbation in DIII-D. *Nuclear Fusion*, 49(5):055027, 2009.

[28] H. Frerichs, O. Schmitz, T. Evans, Y. Feng, and D. Reiter. The pattern of parallel edge plasma flows due to pressure gradients, recycling, and resonant magnetic perturbations in DIII-D. *Physics of Plasmas*, 22(7):–, 2015.

[29] T.E. Evans, D.M. Orlov, A. Wingen, W. Wu, A. Loarte, T.A. Casper, O. Schmitz, G. Saibene, M.J. Schaffer, and E. Daly. 3d vacuum magnetic field modelling of the iter elm control coil during standard operating scenarios. *Nuclear Fusion*, 53(9):093029, 2013.

[30] I.T. Chapman, M. Becoulet, T. Bird, J. Canik, M. Cianciosa, W.A. Cooper, T. Evans, N. Ferraro, C. Fuchs, M. Gryaznevich, Y. Gribov, C. Ham, J. Hanson, G. Huijsmans, A. Kirk, S. Lazerson, Y. Liang, I. Lupelli, R.A. Moyer, C. Nührenberg, F. Orain, D. Orlov, W. Suttrop, D. Yadykin, the ASDEX Upgrade, DIII-D, MAST, NSTX Teams, and EFDA-JET Contributors. Three-dimensional distortions of the tokamak plasma boundary: boundary displacements in the presence of resonant magnetic perturbations. *Nuclear Fusion*, 54(8):083006, 2014.

[31] S A Lazerson and I T Chapman. Stellopt modeling of the 3d diagnostic response in iter. *Plasma Physics and Controlled Fusion*, 55(8):084004, 2013.

[32] J.P. Graves, I.T. Chapman, S. Coda, M. Lennholm, M. Albergante, and M. Jucker. Control of magnetohydrodynamic stability by phase space engineering of energetic ions in tokamak plasmas. *Nat Commun*, 3:624–, January 2012.

[33] O. Schmitz, M. Becoulet, P. Cahyna, T.E. Evans, Y. Feng, H. Frerichs, A. Kirschner, A. Kukushkin, R. Laengner, T. Lunt, A. Loarte, R. Pitts, D. Reiser, D. Reiter, G. Saibene, and U. Samm. Modeling of divertor particle and heat loads during application of resonant magnetic perturbation fields for ELM control in ITER. *Journal of Nuclear Materials*, 438, Supplement(0):S194 – S198, 2013.

[34] A.S. Kukushkin, H.D. Pacher, V. Kotov, G.W. Pacher, and D. Reiter. Finalizing the ITER divertor design: The key role of SOLPS modeling. *Fusion Engineering and Design*, 86(12):2865 – 2873, 2011.

[35] A.S. Kukushkin, H.D. Pacher, A. Loarte, V. Komarov, V. Kotov, M. Merola, G.W. Pacher, and D. Reiter. Analysis of performance of the optimized divertor in ITER. *Nuclear Fusion*, 49(7):075008, 2009.

[36] G. T. A. Huijsmans, C. S. Chang, N. Ferraro, L. Sugiyama, F. Waelbroeck, X. Q. Xu, A. Loarte, and S. Futatani. Modelling of edge localised modes and edge localised mode control. *Physics of Plasmas (1994-present)*, 22(2):–, 2015.

[37] T. Casper, Y. Gribov, A. Kavin, L.E. Lukash, R. Khayrutdinov, H. Fujieda, and C.E. Kessel. Development of the ITER baseline inductive scenarios. *Nuclear Fusion*, 52, 2012. in press.

[38] M. Becoulet, F. Orain, P. Maget, N. Mellet, X. Garbet, E. Nardon, G.T.A. Huysmans, T. Casper, A. Loarte, P. Cahyna, A. Smolyakov, F.L. Waelbroeck, M. Schaffer, T. Evans, Y. Liang, O. Schmitz, M. Beurskens, V. Rozhansky, and E. Kaveeva. Screening of resonant magnetic perturbations by flows in tokamaks. *Nuclear Fusion*, 52(5):054003, 2012.

[39] O. Schmitz, J.W. Coenen, H. Frerichs, M. Kantor, M. Lehnen, B. Unterberg, S. Brezinsek, M. Clever, T. Evans, K.H. Finken, M. Jakubowski, A. Kraemer-Flecken, V. Phillips, D. Reiter, U. Samm, G.W. Spakman, and G. Telesca. Particle confinement control with resonant magnetic perturbations at TEXTOR. *Journal of Nuclear Materials*, 390 - 391(0):330 – 334, 2009.

[40] O. Schmitz, T.E. Evans, M.E. Fenstermacher, M. Lehnen, H. Stoschus, E.A. Unterberg, J.W. Coenen, H. Frerichs, M.W. Jakubowski, R. Laengner, C.L. Lasnier, S. Mordijck, R.A. Moyer, T.H. Osborne, H. Reimerdes, D. Reiter, U. Samm, B. Unterberg, and the DIII-D and TEXTOR teams. Resonant features of energy and particle transport during application of resonant magnetic perturbation fields at TEXTOR and DIII-D. *Nuclear Fusion*, 52(4):043005, 2012.

[41] D. Reiser and D. Chandra. Plasma currents induced by resonant magnetic field perturbations in tokamaks. *Physics of Plasmas*, 16(4):042317, 2009.

[42] Dirk Reiser. Revisited global drift fluid model for linear devices. *Physics of Plasmas (1994-present)*, 19(7):–, 2012.

[43] M. Becoulet, E. Nardon, G. Huysmans, W. Zwingmann, P. Thomas, M. Lipa, R. Moyer, T. Evans, V. Chuyanov, Y. Gribov, A. Polevoi, G. Vayakis, G. Federici, G. Saibene, A. Portone, A. Loarte, C. Doebert, C. Gimblett, J. Hastie, and V. Parail. Numerical study of the resonant magnetic perturbations for type i edge localized modes control in iter. *Nuclear Fusion*, 48(2):024003, 2008.

[44] P. Cahyna, M. Peterka, E. Nardon, H. Frerichs, and R. Panek. Method for comparison of tokamak divertor strike point data with magnetic perturbation models. *Nuclear Fusion*, 54(6):064002, 2014.

[45] N. M. Ferraro. Calculations of two-fluid linear response to non-axisymmetric fields in tokamaks. *Physics of Plasmas*, 19(5):056105, 2012.

[46] F. Orain, M. Bécoulet, G. Dif-Pradalier, G. Huijsmans, S. Pamela, E. Nardon, C. Passeron, G. Latu, V. Grandgirard, A. Fil, A. Ratnani, I. Chapman, A. Kirk, A. Thornton, M. Hoelzl, and P. Cahyna. Non-linear magnetohydrodynamic modeling of plasma response to resonant magnetic perturbations. *Physics of Plasmas (1994-present)*, 20(10):–, 2013.

[47] O. Schmitz, H. Frerichs, M. Becoulet, P. Cahyna, T.E. Evans, Y. Feng, N. Ferraro, G. Huijsmans, M. Lanctot, L. Lao, A. Loarte, R. Pitts, D. Reiser, and D. Reiter. Impact of the plasma response in three-dimensional edge plasma transport modeling for RMP ELM control at ITER. Invited Talk, APS-DPP Meeting, New Orleans, LA, USA, 2014.

[48] A. Wingen, N.M. Ferraro, M.W. Shafer, E.A. Unterberg, T.E. Evans, D.L. Hillis, and P.B. Snyder. Impact of plasma response on plasma displacements in diii-d during application of external 3d perturbations. *Nuclear Fusion*, 54(6):064007, 2014.

[49] M. J. Lanctot, H. Reimerdes, A. M. Garofalo, M. S. Chu, J. M. Hanson, Y. Q. Liu, G. A. Navratil, I. N. Bogatu, Y. In, G. L. Jackson, R. J. La Haye, M. Okayabashi, J.-K. Park, M. J. Schaffer, O. Schmitz, E. J. Strait, and A. D. Turnbull. Measurement and modeling of three-dimensional equilibria in DIII-D. *Physics of Plasmas*, 18(5):056121, 2011.

[50] S R Haskey, M J Lanctot, Y Q Liu, C Paz-Soldan, J D King, B D Blackwell, and O Schmitz. Effects of resistivity and rotation on the linear plasma response to non-axisymmetric magnetic perturbations on diii-d. *Plasma Physics and Controlled Fusion*, 57(2):025015, 2015.

[51] M. Bécoulet, F. Orain, G.T.A. Huijsmans, S. Pamela, P. Cahyna, M. Hoelzl, X. Garbet, E. Franck, E. Sonnendrücker, G. Dif-Pradalier, C. Passeron, G. Latu, J. Morales, E. Nardon, A. Fil, B. Nkonga, A. Ratnani, and V. Grandgirard. Mechanism of edge localized mode mitigation by resonant magnetic perturbations. *Phys. Rev. Lett.*, 113:115001, Sep 2014.

[52] François Orain, M Bécoulet, J Morales, G T A Huijsmans, G Dif-Pradalier, M Hoelzl, X Garbet, S Pamela, E Nardon, C Passeron, G Latu, A Fil, and P Cahyna. Non-linear mhd modeling of edge localized mode cycles and mitigation by resonant magnetic perturbations. *Plasma Physics and Controlled Fusion*, 57(1):014020, 2015.

[53] R. Nazikian, C. Paz-Soldan, D. Callen, J. S. deGrassie, J. D. Eldon, E. Evans, T. M. Ferraro, N. A. Grierson, B. J. Groebner, R. R. Haskey, S. C. Hegna, C. D. King, J. C. Logan, N. R. McKee, G. A. Moyer, R. M. Okabayashi, M. Orlov, D. H. Osborne, T. J-K. Park, L. Rhodes, T. W. Shafer, M. B. Snyder, P. M. Solomon, W. J. Strait, E. and R. Wade, M.˙ Pedestal bifurcation and resonant field penetration at the threshold of edge-localized mode suppression in the diii-d tokamak. *Phys. Rev. Lett.*, 114:105002, Mar 2015.

[54] C. Paz-Soldan, R. Nazikian, R. Haskey, S. C. Logan, N. J. Strait, E. M. Ferraro, N. M. Hanson, J. D. King, J. J. Lanctot, M. A. Moyer, R. M. Okabayashi, J-K. Park, W. Shafer, M. and J. Tobias, B.˙ Observation of a multimode plasma response and its relationship to density pumpout and edge-localized mode suppression. *Phys. Rev. Lett.*, 114:105001, Mar 2015.

[55] Y. Feng, F. Sardei, P. Grigull, K. McCormick, L. Giannone, J. Kisslinger, D. Reiter, Y. Igitkhanov, and U. Wenzel. Modelling of island divertor physics and comparison to W7-AS experimental results. *Journal of Nuclear Materials*, 313–316(0):857 – 862, 2003.

[56] Y. Feng, H. Frerichs, M. Kobayashi, A. Bader, F. Effenberg, D. Harting, H. Hoelbe, J. Huang, G. Kawamura, J. D. Lore, T. Lunt, D. Reiter, O. Schmitz, and D. Sharma. Recent improvements

in the emc3-eirene code. *Contributions to Plasma Physics*, 54(4-6):426–431, 2014.

[57] Y Feng, M Kobayashi, T Lunt, and D Reiter. Comparison between stellarator and tokamak divertor transport. *Plasma Physics and Controlled Fusion*, 53(2):024009, 2011.

[58] D. Reiter, M. Baelmans, and P.Börner. The EIRENE and B2-EIRENE codes. *Fusion Science and Technology*, 47(2):172–186, 2005.

[59] H. Frerichs, D. Reiter, O. Schmitz, T.E. Evans, and Y. Feng. Three-dimensional edge transport simulations for DIII-D plasmas with resonant magnetic perturbations. *Nuclear Fusion*, 50(3):034004, 2010.

[60] H. Frerichs, D. Reiter, O. Schmitz, P. Cahyna, T. E. Evans, Y. Feng, and E. Nardon. Impact of screening of resonant magnetic perturbations in three dimensional edge plasma transport simulations for DIII-D. *Physics of Plasmas*, 19(5):052507, 2012.

[61] H. Frerichs, D. Reiter, O. Schmitz, D. Harting, T.E. Evans, and Y. Feng. On gas flow effects in 3D edge transport simulations for DIII-D plasmas with resonant magnetic perturbations. *Nuclear Fusion*, 52(5):054008, 2012.

[62] Y. Feng, T. Lunt, A. Kukushkin, M. Becoulet, T. Casper, T.E. Evans, H. Frerichs, A. Loarte, R. Pitts, D. Reiter, and O. Schmitz. EMC3-Eirene/SOLPS4.3 comparison for ITER. In *European Conference Abstracts*, volume 35G, 2011. Poster contribution P1.071 on the EPS Conference on Plasma Physics 2011, Strasbourg, France.

[63] M. Kobayashi, Y. Feng, A. Loarte, G. Federici, G. Strohmayer, M. Shimada, F. Sardei, D. Reiter, and M. Sugihara. 3d edge transport analysis of iter start-up configuration for limiter power load assessment. *Nuclear Fusion*, 47(2):61, 2007.

[64] T. Lunt, Y. Feng, M. Bernert, A. Herrmann, P. de Marné, R. McDermott, H.W. Müller, S. Potzel, T. Pütterich, S. Rathgeber, W. Suttrop, E. Viezzer, E. Wolfrum, M. Willensdorfer, and the ASDEX Upgrade team. First emc3-eirene simulations of the impact of the edge magnetic perturbations at asdex upgrade compared with the experiment. *Nuclear Fusion*, 52(5):054013, 2012.

[65] J.D. Lore, J.M. Canik, Y. Feng, J.-W. Ahn, R. Maingi, and V. Soukhanovskii. Implementation of the 3d edge plasma code emc3-eirene on nstx. *Nuclear Fusion*, 52(5):054012, 2012.

[66] M. Kobayashi, S. Morita, C.F. Dong, Z.Y. Cui, Y.D. Pan, Y.D. Gao, H.Y. Zhou, Y. Feng, S. Masuzaki, M. Goto, T. Morisaki, H. Yamada, J. Cheng, P. Sun, Q.W. Yang, X.R. Duan, and the LHD Experiment Group. Edge impurity transport study in the stochastic layer of lhd and the scrape-off layer of hl-2a. *Nuclear Fusion*, 53(3):033011, 2013.

[67] M. Kobayashi, S. Masuzaki, I. Yamada, Y. Narushima, C. Suzuki, N. Tamura, B.J. Peterson, S. Morita, C.F. Dong, N. Ohno, S. Yoshimura, Y. Feng, M. Goto, K. Sato, T. Akiyama, K. Tanaka, and the LHD experiment group. Control of 3D edge radiation structure with resonant magnetic perturbation fields applied to the stochastic layer and stabilization of radiative divertor plasma in LHD. *Nuclear Fusion*, 53(9):093032, 2013.

[68] H. Frerichs and D. Reiter. Stability and control of iterated non-linear transport solvers for fusion edge plasmas. *Computer Physics Communications*, 188(0):82 – 87, 2015.

[69] M. E. Fenstermacher, T. E. Evans, T. H. Osborne, M. J. Schaffer, M. P. Aldan, J. S. deGrassie, P. Gohil, I. Joseph, R. A. Moyer, P. B. Snyder, R. J. Groebner, M. Jakubowski, A. W. Leonard, O. Schmitz, and the DIII-D Team. Effect of island overlap on edge localized mode suppression by resonant magnetic perturbations in DIII-D. *Physics of Plasmas*, 15(5):056122, 2008.

[70] H. Frerichs, M. Clever, Y. Feng, M. Lehnen, D. Reiter, and O. Schmitz. Numerical analysis of particle recycling in the TEXTOR helical divertor. *Nuclear Fusion*, 52(2):023001, 2012.

[71] Alberto Loarte. Effects of divertor geometry on tokamak plasmas. *Plasma Physics and Controlled Fusion*, 43(6):R183, 2001.

[72] T. Eich, B. Sieglin, A. Scarabosio, W. Fundamenski, R. J. Goldston, and A. Herrmann. Inter-ELM power decay length for JET and ASDEX upgrade: Measurement and comparison with heuristic drift-based model. *Phys. Rev. Lett.*, 107:215001, Nov 2011.

[73] R.J. Goldston. Heuristic drift-based model of the power scrape-off width in low-gas-puff H-mode

tokamaks. *Nuclear Fusion*, 52(1):013009, 2012.

[74] E.A. Unterberg, T.E. Evans, R. Maingi, N.H. Brooks, M.E. Fenstermacher, S. Mordijck, and R.A. Moyer. Demonstration of particle exhaust control during ELM suppression by resonant magnetic perturbations in DIII-D. *Nuclear Fusion*, 49(9):092001, 2009.

[75] T. Lunt, Y. Feng, E. Wolfrum, S. Potzel, S.K. Rathgeber, W. Suttrop, , and the ASDEX Upgrade Team. EMC3-Eirene simulations of the impact of Magnetic Perturbations on the neutral particle recycling in ASDEX Upgrade. In *EPC Conference Abstracts, P4.107*, 2013. 40th EPS Conference on Plasma Phsyics.

[76] J.W. Coenen, O. Schmitz, B. Unterberg, M. Clever, M.A. Jakubowski, U. Samm, B. Schweer, H. Stoschus, M. Tokar, and the TEXTOR-Team. Rotation and radial electric field in the plasma edge with resonant magnetic perturbation at TEXTOR. *Nuclear Fusion*, 51(6):063030, 2011.

[77] S. Mordijck, R.A. Moyer, N.M. Ferraro, M.R. Wade, and T.H. Osborne. The radial electric field as a measure for field penetration of resonant magnetic perturbations. *Nuclear Fusion*, 54(8):082003, 2014.

[78] G.R. McKee, Z. Yan, C. Holland, R.J. Buttery, T.E. Evans, R.A. Moyer, S. Mordijck, R. Nazikian, T.L. Rhodes, O. Schmitz, and M.R. Wade. Increase of turbulence and transport with resonant magnetic perturbations in elm-suppressed plasmas on diii-d. *Nuclear Fusion*, 53(11):113011, 2013.

[79] J.D. Callen. Effects of 3D magnetic perturbations on toroidal plasmas. *Nuclear Fusion*, 51(9):094026, 2011.

[80] J.D. Callen, C.C. Hegna, and A.J. Cole. Magnetic-flutter-induced pedestal plasma transport. *Nuclear Fusion*, 53(11):113015, 2013.

[81] V. A. Soukhanovskii, R. E. Bell, A. Diallo, S. Gerhardt, S. Kaye, E. Kolemen, B. P. LeBlanc, A. G. McLean, J. E. Menard, S. F. Paul, M. Podesta, R. Raman, T. D. Rognlien, A. L. Roquemore, D. D. Ryutov, F. Scotti, M. V. Umansky, D. Battaglia, M. G. Bell, D. A. Gates, R. Kaita, R. Maingi, D. Mueller, and S. A. Sabbagh. Snowflake divertor configuration studies in national spherical torus experiment. *Physics of Plasmas*, 19(8):082504, 2012.

[82] M. Kotschenreuther, P. Valanju, S. Mahajan, L.J. Zheng, L.D. Pearlstein, R.H. Bulmer, J. Canik, and R. Maingi. The super x divertor (sxd) and a compact fusion neutron source (cfns). *Nuclear Fusion*, 50(3):035003, 2010.

[83] A. Kirschner, V. Philipps, J. Winter, and U. Kögler. Simulation of the plasma-wall interaction in a tokamak with the Monte Carlo code ERO-TEXTOR. *Nuclear Fusion*, 40(5):989, 2000.

[84] A. Kirschner, D. Borodin, S. Droste, V. Philipps, U. Samm, G. Federici, A. Kukushkin, and A. Loarte. Modelling of tritium retention and target lifetime of the ITER divertor using the ERO code. *Journal of Nuclear Materials*, 363–365(0):91 – 95, 2007.

[85] T. E. Evans and D. F. Finkenthal. Monte Carlo impurity transport modeling in the DIII-D Tokamak. *AIP Conference Proceedings*, 443(1):58–72, 1998.